FTL REPORT R86-8

FLIGHT TESTS OF A DIGITAL DATA ACQUISITION SYSTEM

FOR ANALYSIS OF ULTRASONIC PULSE-ECHO SIGNALS

USED TO MEASURE ICE ACCRETION

JUSTIN M. RYAN, JR.
AND
R. JOHN HANSMAN, JR.

MAY 1986

FLIGHT TRANSPORTATION LABORATORY REPORT R86-8

FLIGHT TESTS OF A DIGITAL DATA ACQUISITION SYSTEM

FOR ANALYSIS OF ULTRASONIC PULSE-ECHO SIGNALS

USED TO MEASURE ICE ACCRETION

Justin Mark Ryan, Jr.

and

R. John Hansman, Jr.

May 1986

FTL REPORT R86-8

FLIGHT TESTS OF A DIGITAL DATA ACQUISITION SYSTEM FOR ANALYSIS OF ULTRASONIC PULSE-ECHO SIGNALS USED TO MEASURE ICE ACCRETION

ABSTRACT

A number of signal processing algorithms were developed for analyzing ultrasonic signals used to measure aircraft ice accretion in flight. A high speed digital signal acquisition system was designed and constructed to acquire the signals. The ultrasonic signals were acquired during a series of flight tests in actual icing conditions. This digital data was used to evaluate various algorithms for determining the ice thickness. An analog data acquisition system provided data for comparison with the digital data. A gated peak detector, employing low signal to noise ratio filtering and derivative preprocessing, was developed. This algorithm correctly determined the ice thickness for all tested flight data. Icing rate algorithms were also developed. The measured icing rate correlated reasonable well with the liquid water content of the cloud.

ACKNOWLEDGMENTS

TABLE OF CONTENTS

1. INTRODUCTION

This thesis focuses on the development of signal
processing algorithms for analyzing ultrasonic signals
used to measure aircraft ice accretion in flight. The
ultrasonic signals were collected during a series of
flight tests in actual icing conditions. A number of
signal processing algorithms were evaluated using these
signals. Chapter 1 contains an explanation of the need
for icing measurement systems, a description of the
ultrasonic technique, and an outline of the ultrasonic
signal characteristics. Chapter 2 contains a description
of the digital and analog systems used to collect the
ultrasonic signals during the flight tests. The flight
test data and the signal processing results are described
in Chapter 3. Chapter 4 contains conclusions about the
performance of the various signal processing algorithms.

1.1 ICING MEASUREMENT

Icing measurement systems are important for a variety
of reasons. First, as part of the caution and warning
system on an aircraft, they can help pilots minimize
exposure to severe icing conditions. Due to the expense
of ice protection systems, only about ten percent of civil
aircraft have any means to prevent icing or remove
accreted ice, making avoidance important. While a pilot
can visually observe that icing is occuring, he cannot
determine how much ice has accreted on surfaces out of

view. Quickly determining the severity is also difficult. An inexpensive detection and measurement system could aid the pilot in seeking less severe conditions and would improve the safety of these aircraft.

Second, icing measurement systems can serve in automatic control systems for ice protection equipment. The current and proposed methods for removing ice, such as pneumatic boots or electro-impulse de-icing are most efficient over a restricted ice thickness range. An effective control system requires a reliable measure of the ice thickness. And finally, the performance of new aircraft, with more advanced wing designs, are expected to be more sensitive to icing, also requiring an accurate measurement system.

1.2   ULTRASONIC MEASUREMENT TECHNIQUE

1.2.1   THEORY

The ultrasonic ice measurement technique, developed at MIT,[1] uses the time of flight for a sound wave travelling through the ice to determine the ice thickness. Figure 1 depicts the technique. A small ultrasonic transducer, typically 1/4 inch in diameter, is mounted flush with the aircraft surface (it could be the wing, rotor, engine inlet, or any other surface of interest). The transducer (a piezioelectric crystal) is excited with a voltage pulse, causing it to emit a compressive wave into the ice. The wave travels through the ice and is

reflected at the ice/air interface. The reflected wave induces an echo voltage pulse in the transducer. The thickness of the ice, D, is related to the time between the pulse and the echo, T_{p-e}, by the formula:

$$D = C \cdot T_{p-e}/2 \qquad\qquad (1)$$

Where C is the propagation speed of the wave through the ice. Previous work[2] has demonstrated that the speed of propagation is insensitive to the various types of ice accreted during flight (rime, glaze, or mixed); a value of 3.8 millimeters per microsecond was used for the results presented in this paper.
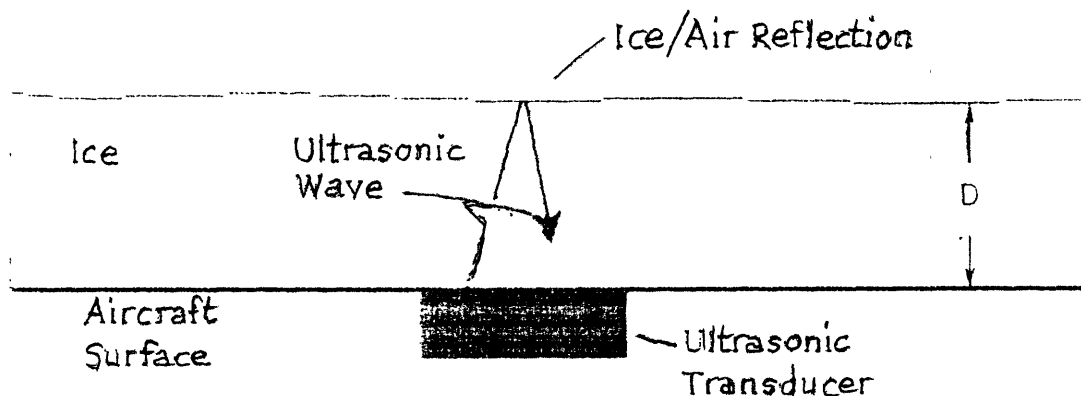

Figure 1: Ultrasonic Ice Thickness Measurement

The physical properties of the piezioelectric
transducer determine the available resolution. A heavily
damped, broadband transducer gives a short pulse width,
while a transducer with a high center frequency results in
a short pulse wavelength. Assuming that the phase of the
echo is not measured, the theoretical resolution of the
ultrasonic technique is half of the pulse wavelength. The
transducers used in this thesis had a 5 Mhz center
frequency, corresponding to a theoretical resolution of
0.38 mm.

1.2.2 COMPARISON OF ULTRASONIC AND PROBE TECHNIQUES

The ultrasonic technique measures the thickness of the
ice directly above the surface mounted transducer. Most
previous ice detection methods measure the mass of the ice
that forms on an externally mounted probe.[3,4] Surface
detectors have an inherent advantage over probe methods
for some applications because ice tends to accrete
differently on a probe than on other surfaces.[5] A small
probe collects more ice than larger bodies (such as a
wing) because it disturbs the flow less (fewer water
droplets are deflected away from the probe by the flow).
Further, the ratio of ice collected by the probe versus a
wing depends on the cloud conditions (the flow has a
greater affect on smaller droplets). While probe methods
may accurately measure the ice on the probe, the icing on
other surfaces must be inferred from this measurement and
may not be accurate. The ultrasonic technique allows a

direct measurement of the ice thickness on any critical surface. Further, multiple probes can be multiplexed in a single ultrasonic system allowing icing mesurements on several critical surfaces.

1.3 ULTRASONIC SIGNAL CHARACTERISTICS
1.3.1 SIGNAL GENERATION

The ultrasonic transducer is typically connected to a pulser-receiver unit through a single cable, as shown in Figure 2. The pulser-receiver generates the outgoing pulse to the piezioelectric transducer and amplifies the return echo. Figure 3 shows a typical voltage signal from the pulser-receiver when the transducer is covered with ice. The first peak in the voltage is the pulse, and the second is the echo. The time between the peaks is the pulse-echo time that corresponds to the ice thickness.

The electrical characteristics of the pulser-receiver affect the characteristics of the ultrasonic signal. The most important electrical characteristics are the damping and gain of the pulser-receiver. The damping matches the impedance of the pulser-receiver to that of the transducer and transmission line. A mismatch from insufficient damping will cause an excessive pulse length and reduce the thickness resolution. Excessive damping causes a reduction in the echo magnitude, decreasing the signal to noise ratio. The gain of the receiver is critical because the echo magnitude must be within the dynamic range of the
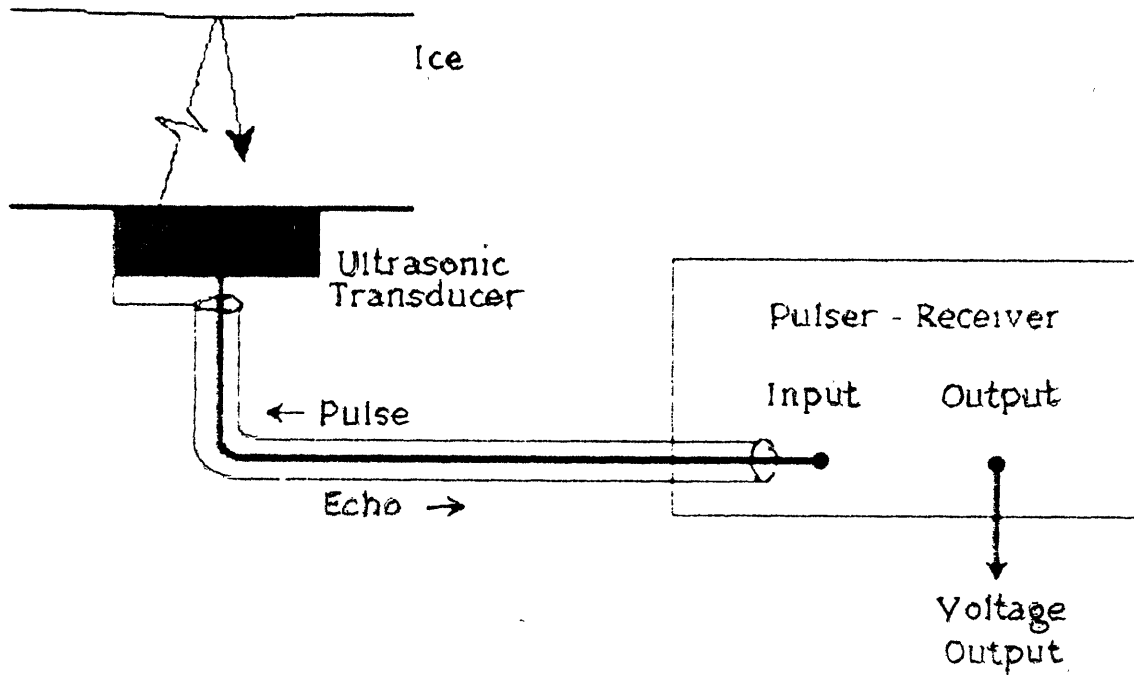
signal acquisition system.

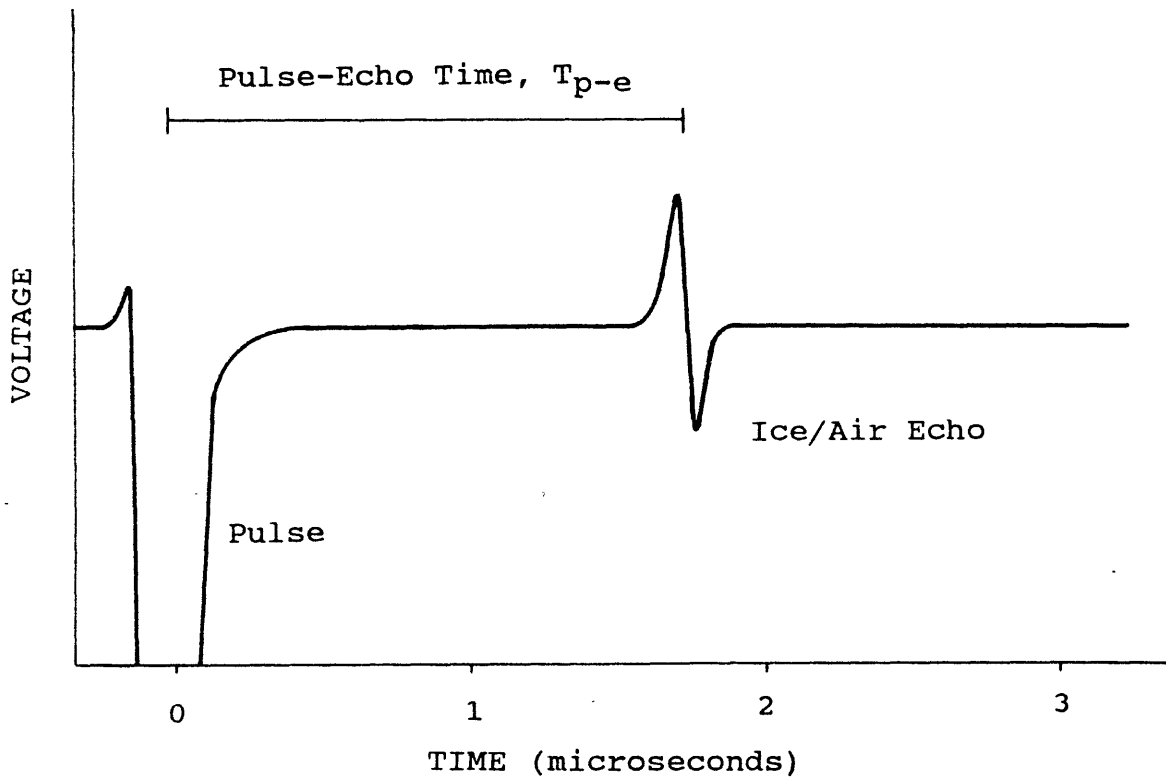Figure 2: Transducer with Pulser-Receiver

Figure 3: Typical Ultrasonic Signal

The outgoing voltage pulse (about 250 volts) causes
the receiver amplifiers to saturate for a few micro-
seconds. If the pulse-echo time is short, as with thin
ice, the echo may be obscured in the saturation region.
The use of an ultrasonic delay line solves this problem by
delaying the return echo. The delay line is a piece of
plexiglass between the transducer and the ice as Figure 4
shows. Figure 5 illustrates a typical signal from a
delay line transducer. The saturation region of the
receiver amplifier ends before the echo returns from the
plexiglass/ice interface. With the delay line, T_{p-e}
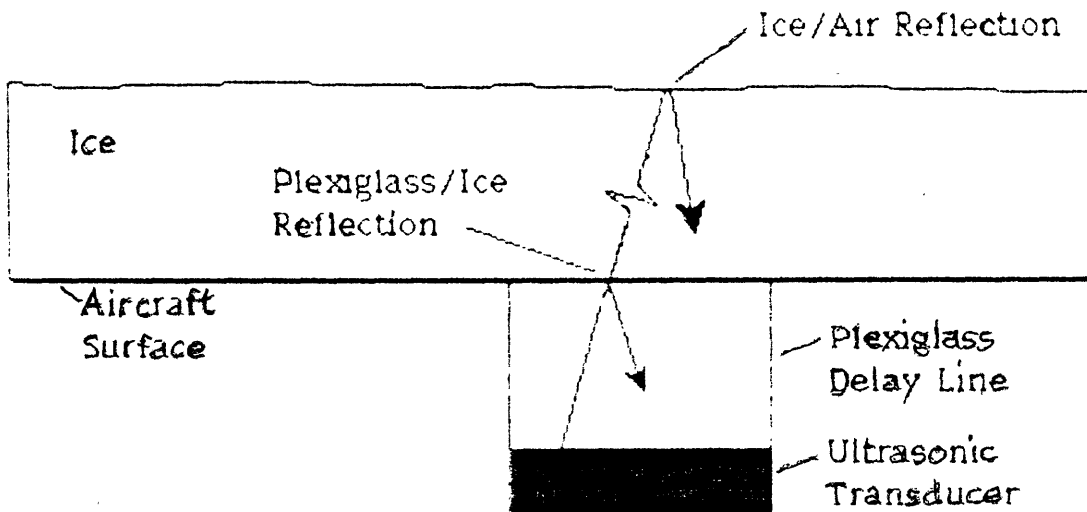becomes the time between the plexiglass/air echo and the
ice/air echo.
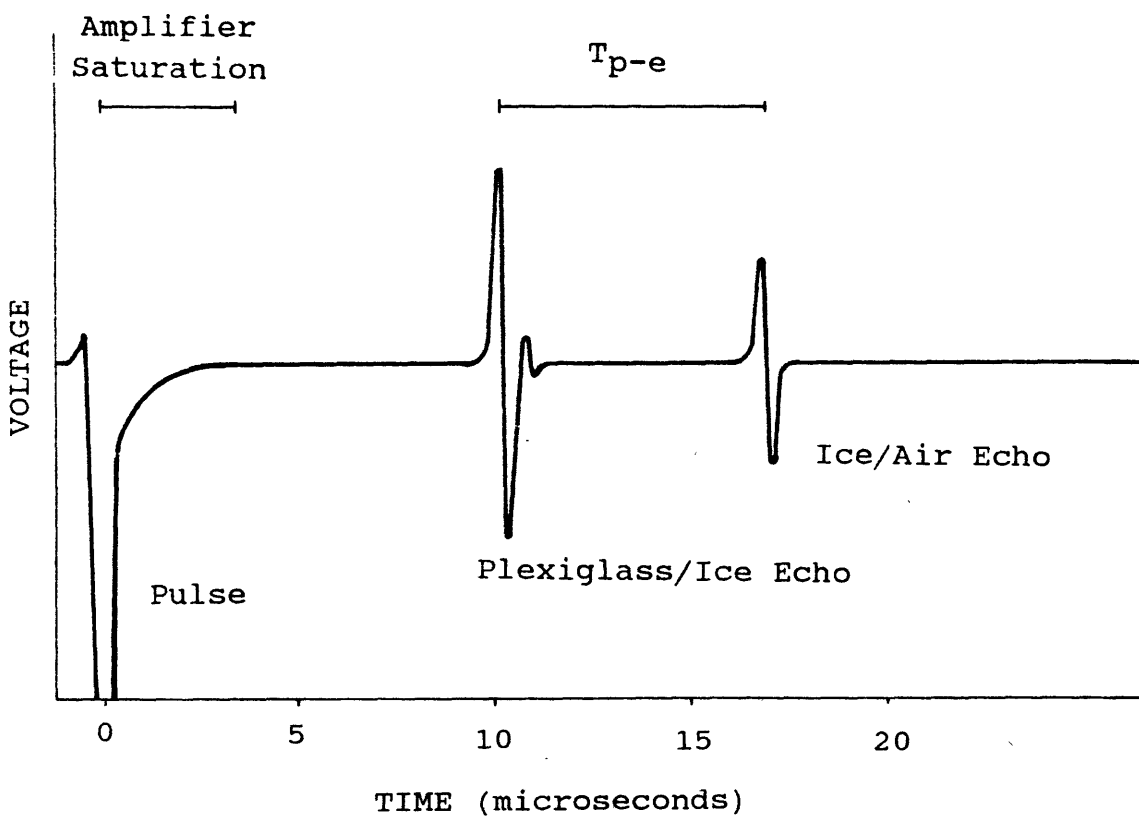
Figure 4: Transducer with Delay Line

TIME (microseconds)

Figure 5: Ultrasonic Signal with Delay Line

1.3.2 SIGNAL ACQUISITION REQUIREMENTS

The requirements for aquiring the ultrasonic signals are driven by their time characteristics. Icing is a relatively slow process, requiring a measurement once every few seconds. The time between the pulse emission and the echo return for typical ice thicknesses is much shorter, ranging from about 1 to 20 microseconds. The cycle period of the ultraound is even shorter, at about 200 nanoseconds (5 Mhz). In order to store the entire waveform, a high bandwidth signal aquisition system is required.

To meet this bandwidth requirement, prior work on ultrasonic ice detectors used videotape storage of the traces from a high bandwidth oscilloscope. The signals were manually processed post-flight by viewing the tapes. Signals aquired using this method could not be processed automatically. The evaluation of automatic signal processing algorithms for this thesis required the development of a high speed digital signal aquisition system. The system had to store a large number of waveforms from the flight tests in digital from in order to evaluate candidate signal processing algorithms using a computer.

The digital signal aquisition system was designed to meet the following specifications (summarized in Table 1): It had to sample the ultrasonic signal at a high enough

rate and with enough magnitude resolution to adequately represent the high frequency components of the signal; a sampling rate of 50 Mhz (ten times the transducer center frequency) at a resolution of 6 bits (64 descrete values) was deemed sufficient. The system had to take enough samples at this rate of the waveform to allow a reasonable pulse-echo time and therefore ice thickness; 1000 samples per waveform, corresponding to a pulse-echo time of 20 microseconds, and a maximum thickness of 38 millimeters, was chosen. And finally, the system had to store complete waveforms at small enough intervals to allow reasonable time resolution of the ice thickness measurements; a 10 second interval was selected, with two waveforms stored after each interval (for redundancy and comparison). The digital signal aquisition system that was designed to meet these requirements is described in Section 2.2.

Table 1: Digital Signal Aquisition System Requirements

1.   50 Mhz sampling rate.

2.   6 bit sample resolution.

3.   1000 samples per waveform.

4.   10 second interval between
      set of 2 waveforms.

The above requirements were necessary for the development of signal processing algorithms. However, an operational system could be much simpler because it may not need to store the entire signal.

1.3.3   SIGNAL PROCESSING REQUIREMENTS

The algorithms used to process the ultrasonic signals must be able to determine the thickness of the ice for a number of different icing formations. Figures 6, 7 and 8 show how the signal characteristics can vary in different icing conditions. Figure 6 illustrates cold, dry icing conditions, where all the supercooled cloud droplets freeze upon impact with the accreting surface. Dry growth results in a smooth ice surface with a strong, short duration echo. Figure 6 also shows the attenuation of the echo in thick ice due to the increased path length of the wave. In warmer conditions, not all the droplets freeze immediately, causing a layer of water to form on the ice surface. The wet growth case, shown in Figure 7, generally results in a rough surface causing a less powerful echo with a longer duration. Figure 8 shows how a layer discontinuity in the ice may cause an echo with a larger magnitude than the ice/air echo. The reflection from the layer is weaker, but the ice/air echo experiences greater attenuation due to the longer path length in the ice. Ultrasonic signal processing algorithms must be able to determine the thickness of dry, wet, and layered ice growths of varied thickness.
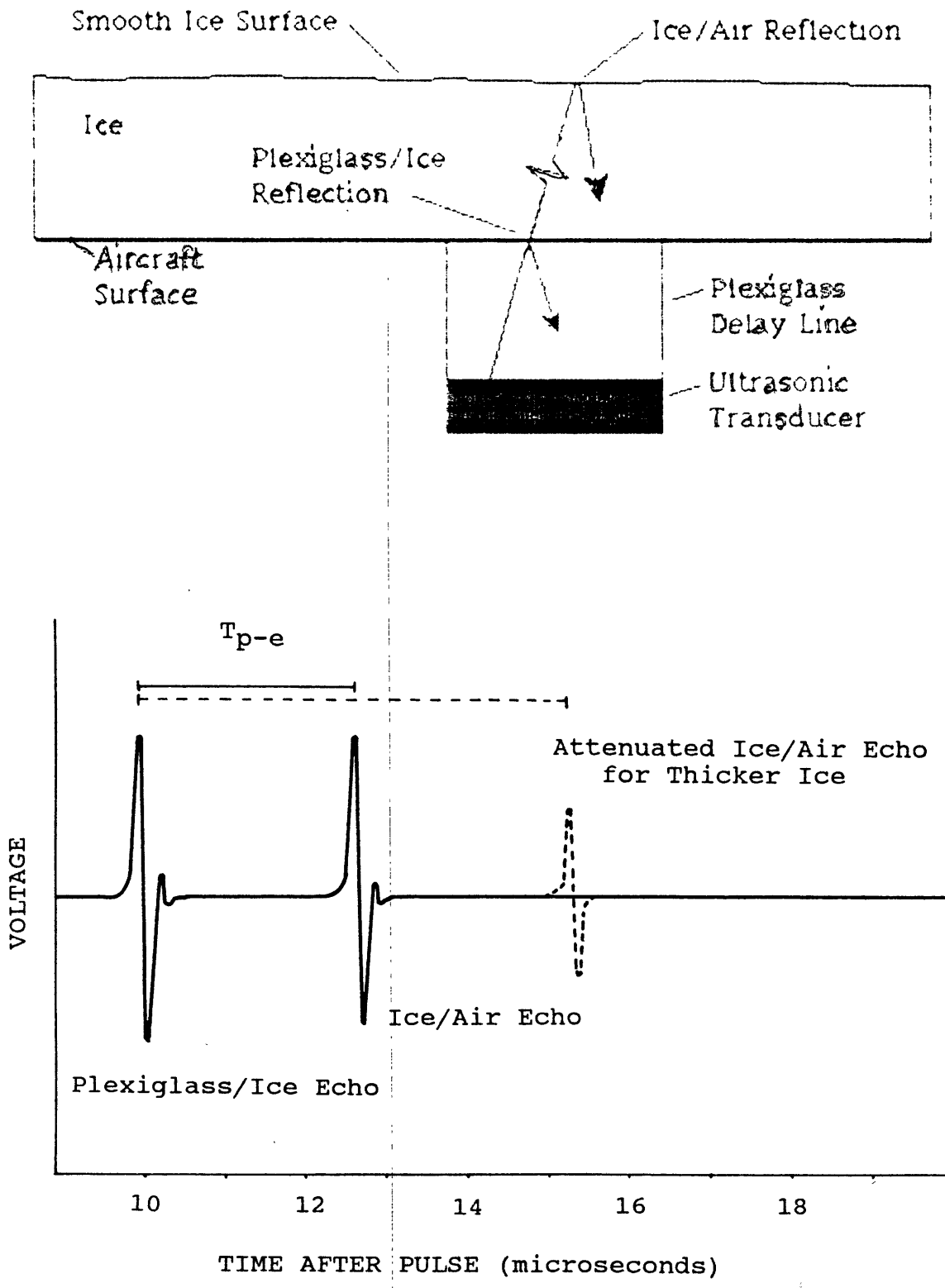
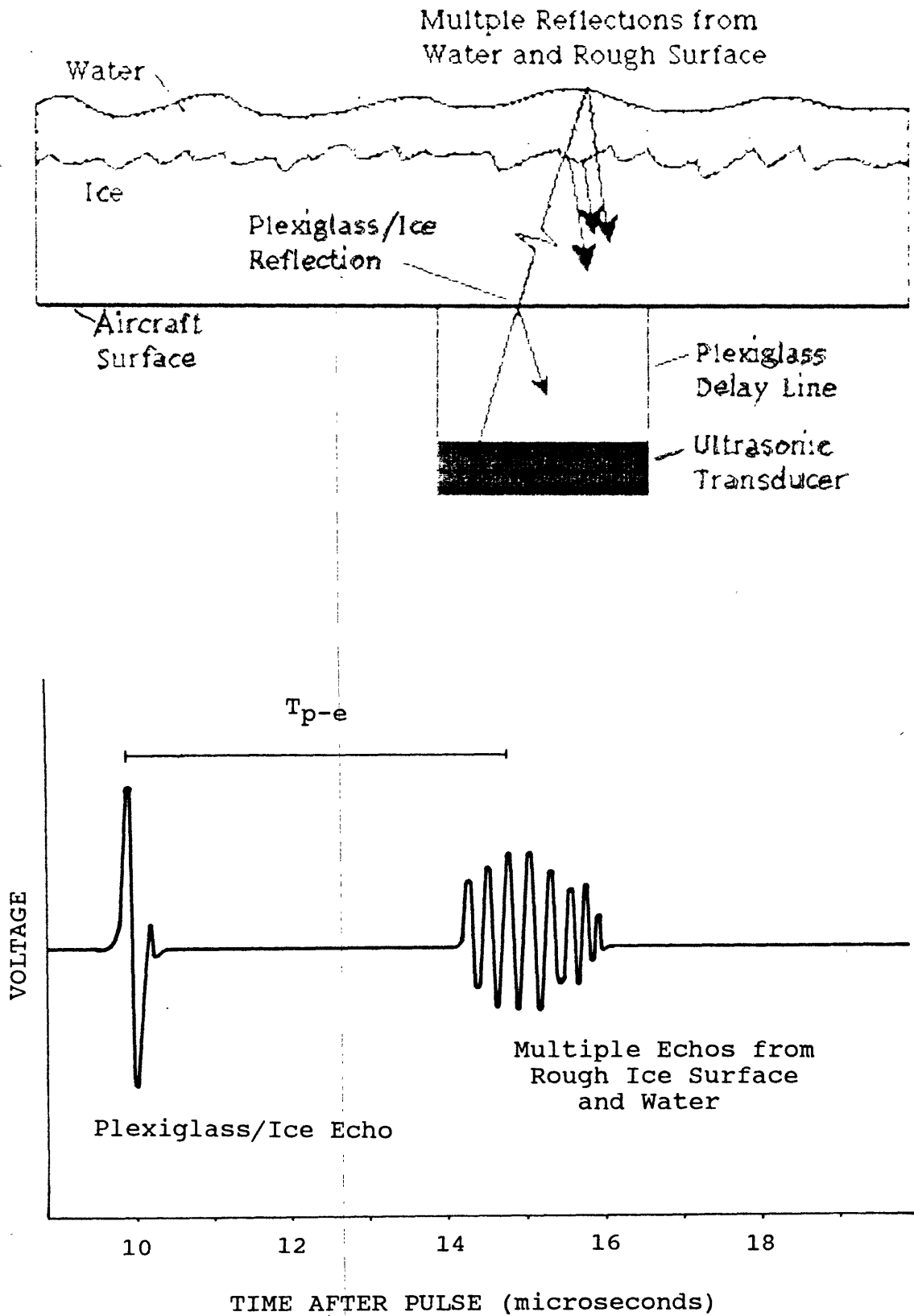Figure 6: Ultrasonic Signal for Dry Ice Growth

Multple Reflections from
Water and Rough Surface

Water

Ice

Plexiglass/Ice
Reflection

Aircraft
Surface

Plexiglass
Delay Line

Ultrasonic
Transducer

T_{p-e}

VOLTAGE

Plexiglass/Ice Echo

Multiple Echos from
Rough Ice Surface
and Water

10   12   14   16   18

TIME AFTER PULSE (microseconds)

Figure 7: Ultrasonic Signal for Wet Ice Growth
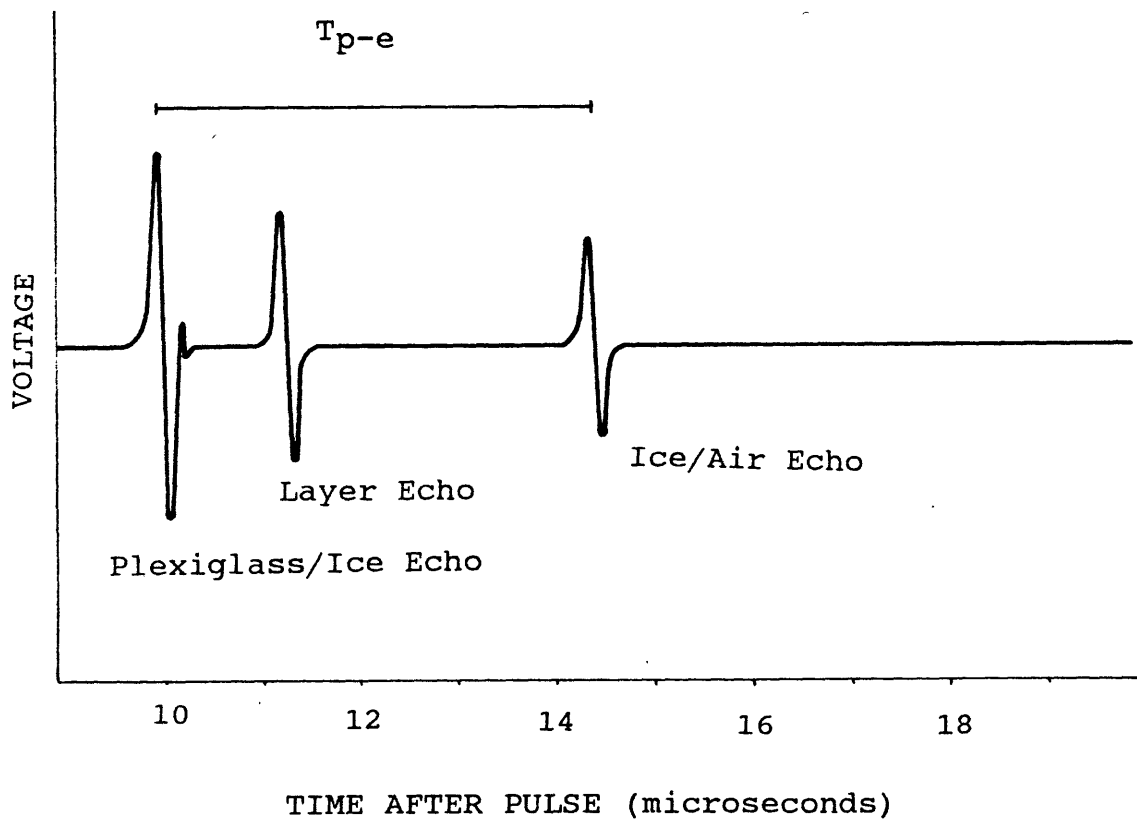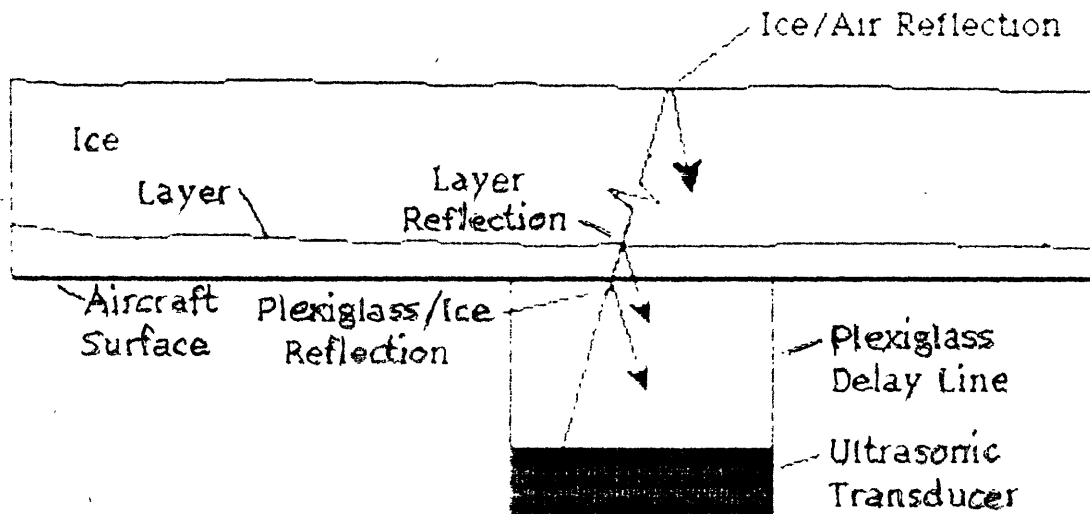
Figure 8: Ultrasonic Signal for Layered Ice Growth

2. EXPERIMENTAL APPARATUS AND METHODS

The purpose of the tests described in this section was to obtain ultrasonic signals during flight in natural icing conditions, so that appropriate signal processing algorithms could be evaluated. Figure 9 is a block diagram of the equipment installed in the test aircraft. The ultrasonic transducers were mounted in the leading edge of the wing. The primary ultrasonic waveform data was stored by a high speed digital signal acquisition system on magnetic tape. After each test flight, the digital data was loaded into a computer for algorithm development and testing. In addition, an analog system used videotape to store oscilloscope traces of the ultrasonic signals. The videotapes were reduced visually for comparison with the digital data. Because the section of the wing with the transducers was not de-iced, the ice remained on the wing after landing, allowing mechanical measurements of the final ice thickness. The mechanical measurements provided a final verification of the ultrasonic data. The next sections describe the signal acquisition systems, the flight test installation, and the flight test procedures.
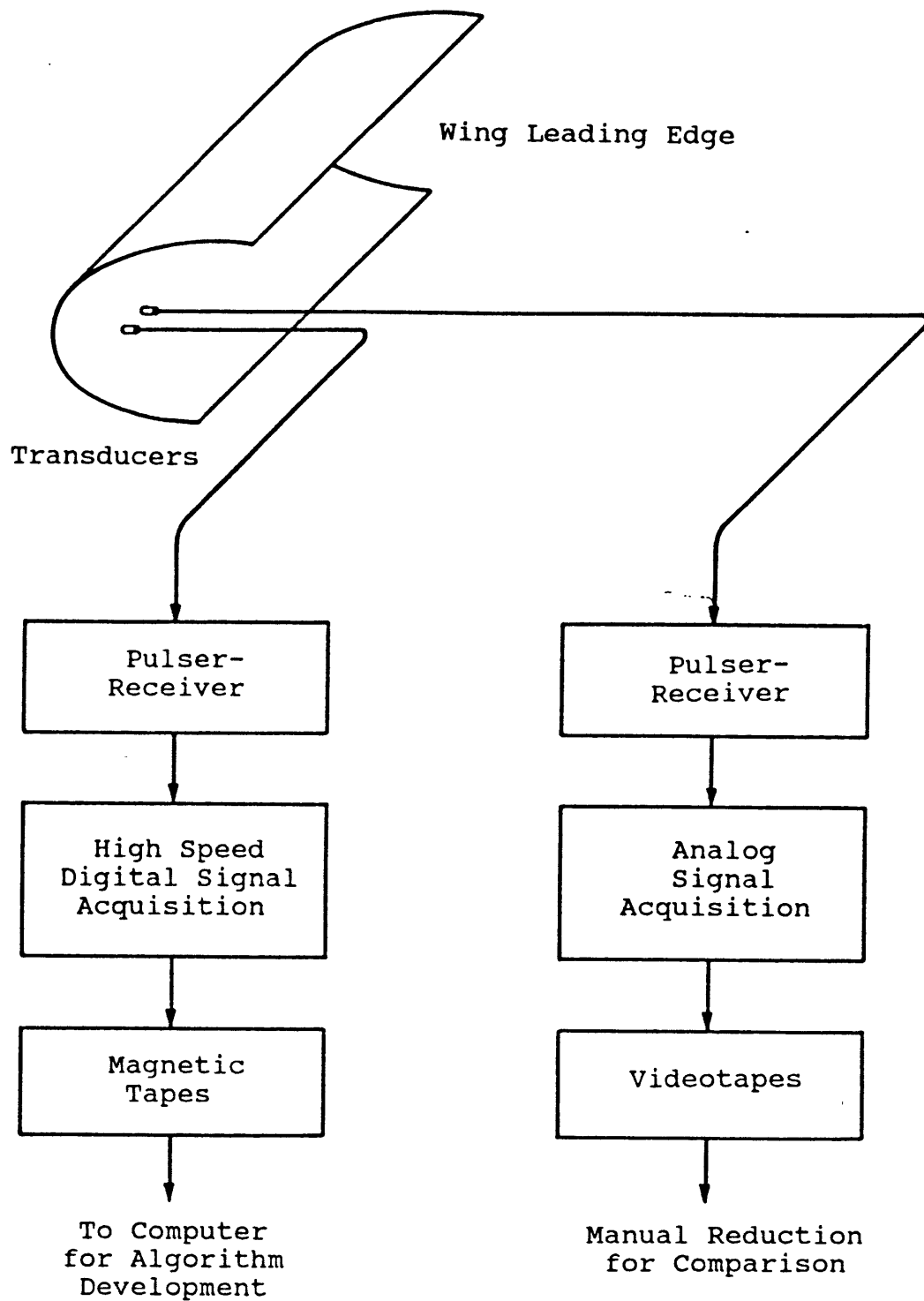
Figure 9: Experimental Apparatus

2.1 DIGITAL SIGNAL ACQUISITION SYSTEM

The digital signal aquisition system was designed to
meet the specifications outlined in Section 1.3.2 and
Table 1. Waveforms aquired by this system were later used
to develop signal processing algorithms. Figure 10 is a
diagram of the system. The ultrasonic transducer was
mounted in the leading edge of the aircraft wing. The
pulser-receiver generates the pulse and amplifies the
return echo. The high speed digitizer and controller is
the heart of the system. It triggers the pulser-receiver,
digitizes the ultrasonic signals at high speed, and stores
the entire wavefrom internally. The digitized signal is
then sent to a tape deck. The data on the tape is later
loaded into a computer on the ground for post-flight
processing.

The high speed digitizer and controller was designed
and constructed as part of this thesis. It is further
descibed in the next section. The transducer, the
pulser-receiver, and the tape deck were "off the shelf"
components. The transducer was a broadband, 5 Mhz center
frequency, 1/4 inch diameter model, with a 10 microsecond
delay line. The pulser-receiver had variable settings for
gain, damping, and pulse energy. The tape deck received
data in 8-bit parallel format and stored it on miniature
magnetic tapes at about 104 kbytes per side. At 2 kbytes
of data stored every 10 seconds, the tapes lasted about 9
minutes per side. The specifications for the transducer,

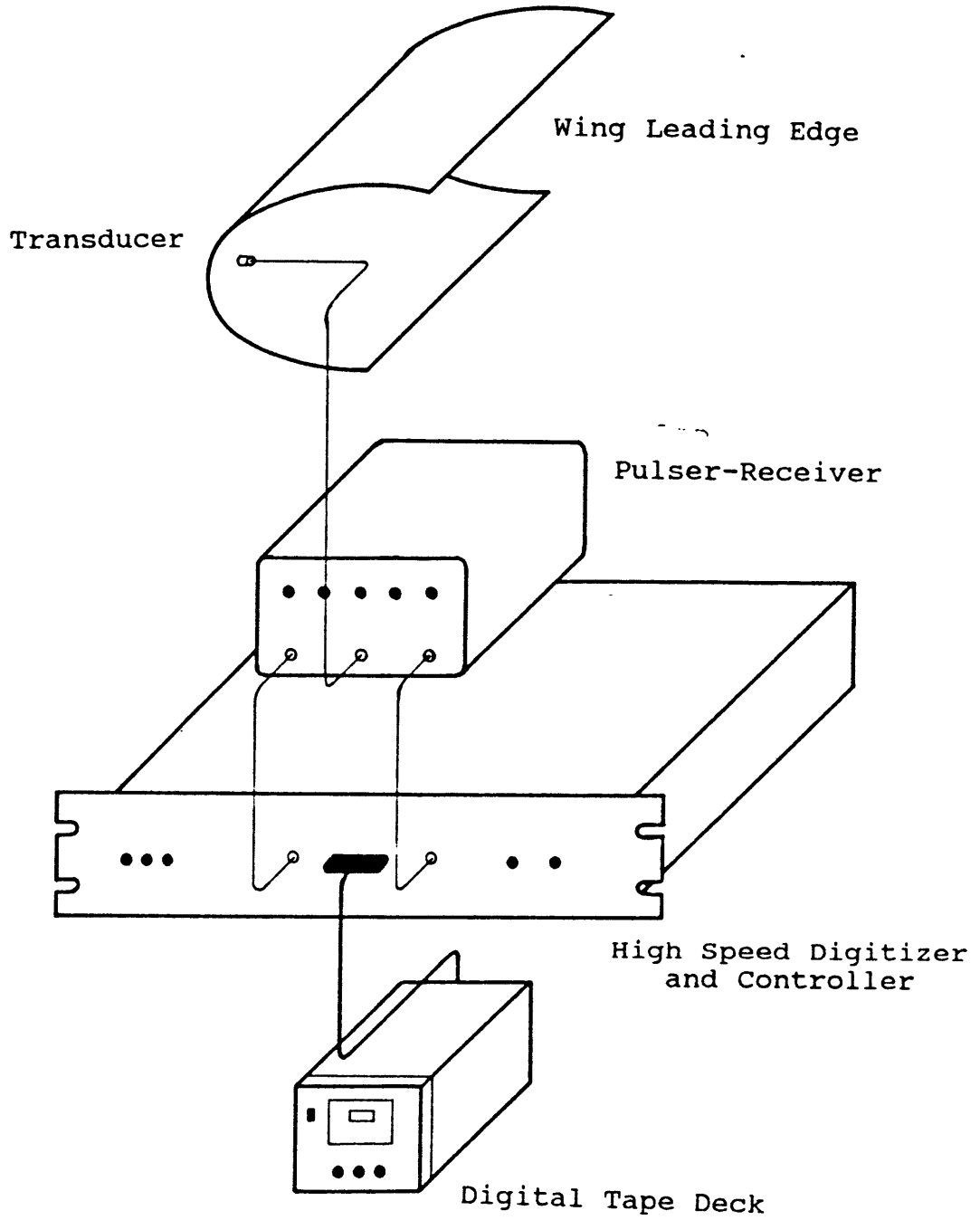the pulser-receiver and the tape deck are given in

Appendix A.

Figure 10: Digital Signal Aquisition System

2.2 HIGH SPEED DIGITIZER AND CONTROLLER

The digitizer triggers the pulser-receiver, digitizes the ultrasonic trace, and sends the data to the tape deck. The complex design was driven by the specifications of 6-bit resolution at 50 Mhz and storage of 1000 points at that rate. The sampling rate of 50 Mhz is near the state of the art for single chip analog to digital converters, and there are no single chip memories that can store 1000 6-bit data points at that rate. Digital circuits at this speed are strongly affected by wire length, stray capacitance, crosstalk, and noise (50 Mhz is a radio frequency). Debugging circuits at 50 Mhz is very difficult because even the highest speed oscilloscopes have trouble displaying 50 Mhz square waves (the first harmonic of a 50 Mhz square wave is at 150 Mhz). Additionally, the high speed digitizer and controller had to operate with three different clocks: a 50 Mhz clock for sampling and storing the signals, a 1 Mhz clock for sending data to the tape deck, and a 10 second clock for controlling the waveform storage interval.

Figure 11 is a block diagram of the high speed digitizer and controller. A brief description of the signal path is followed by a more detailed description of each section of the circuit. A detailed circuit diagram of the digitizer and controller is contained in Appendix A.
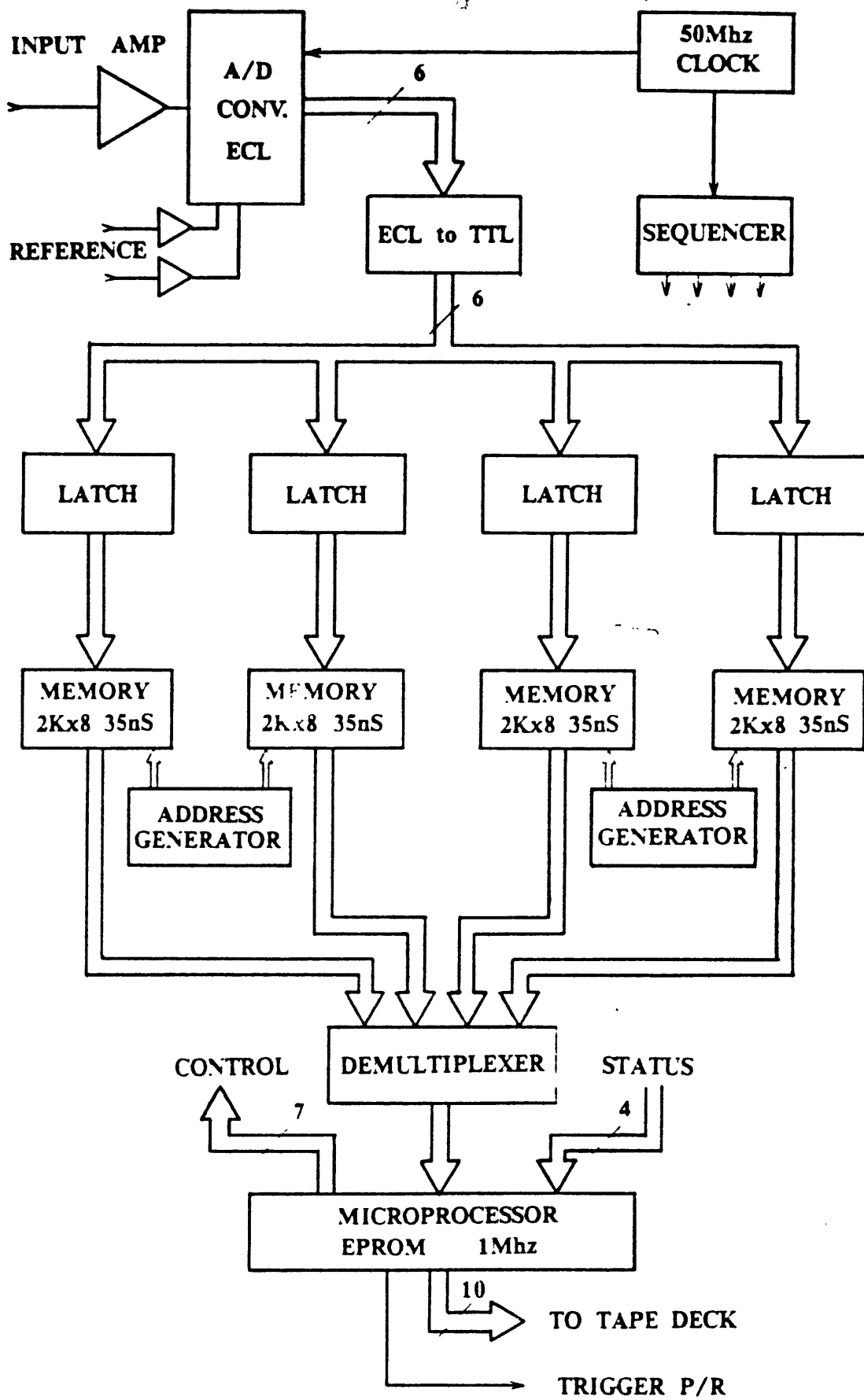
Figure 11: High Speed Digitizer and Controller
Block Diagram

The signal path in Figure 11 flows from the top of the page to the bottom. The ultrasonic signal output from the pulser-receiver was connected to the input amplifier and the analog to digital converter (A/D). The A/D converter sampled the signal at 50 Mhz with 6-bits of resolution. Each 6-bit sample was latched by one of the four latches and stored in the corresponding memory. Since each memory only stored every fourth point, they operated at 12.5 Mhz. Once 2000 points (two complete waveforms) were stored in the memories, the data was demultiplexed and sent through the microprocessor to the tape deck. The operation of each section is described below.

The A/D converter was the highest speed 6-bit single chip converter available when the circuit was designed.[6,7] It had a 7 nanosecond conversion time and could operate at 100 Mhz. To achieve this performance the chip used Emmiter Coupled Logic (ECL) and a "flash" conversion technique (64 high speed comparitors connected to a resistor network). The A/D converter input was internally connected directly to the comparitors, placing stringent demands on the input amplifier. The amplifier had to drive a largely capacitive load at high frequency and offset the input voltage to the correct range (-1.3 to -.3 volts). The operational amplifier chosen for the input amplifier was also a state of the art design, with a 65 Mhz bandwidth independant of gain.[8] The output of the A/D converter was ECL (-5 or 0 volts) and required translation

to TTL (+5 or 0 volts) for compatibility with the rest of
the components which were FAST TTL (except the memories,
which were TTL compatible CMOS).

The sequencer controled the multiplexing of the data
into the memories. It generated four sequential 12.5 Mhz
control lines that were connected to the latches, the
memories, and the address generators. It also controled
the demultiplexer when the data was read from the
memories. During the read operation the sequencing rate
was determined by the microprocessor (described later).

The memories were very fast 2k by 8-bit CMOS static
RAMs (random access memories). The access time of 35
nanoseconds was the fastest available for memories of this
size.[9] While these memories provided more storage space
than necessary, other memory choices would have increased
the number of chips required.

The address generators produced the 11-bit (2k)
addresses for the memories. The time to increment the
addresses required the use of two generators (one
generator incremented while the opposite memories were
storing).

The demultiplexer put the data in the correct order
when it was read from the memories. It was controled by
the sequencer.

The microprocessor shown in Figure 11 performed a
variety of functions: it triggered the pulser-receiver;
started and stoped the storage of data by the digitizer;
and fed the data to the tape deck.   Figure 12 shows the
flowchart for the microprocessor program (stored in an
EPROM).   The microprocessor controlled the storage of data
using 7 control lines and 4 status lines.   A 10 second
clock connected to the microprocessor provided the
waveform storage interval (a 5 second clock was also
installed but was not used on any of the flights since the
tapes had a limited capacity and would only last 4 minutes
at this interval).   A 9 microsecond delay after the
trigger insured that the plexiglass/ice echo, which occurs
10 microseconds after the pulse, was stored.   A front
panel reset switch started the system.   An LED on the
front panel was illuminated at every trigger so that the
time of the trigger for the first wavefrom on each tape
could be recorded (times for each successive waveform
could be determined assuming a fixed 10 second interval).

The circuit diagram for the high speed digitizer and
controller is contained in Appendix A.
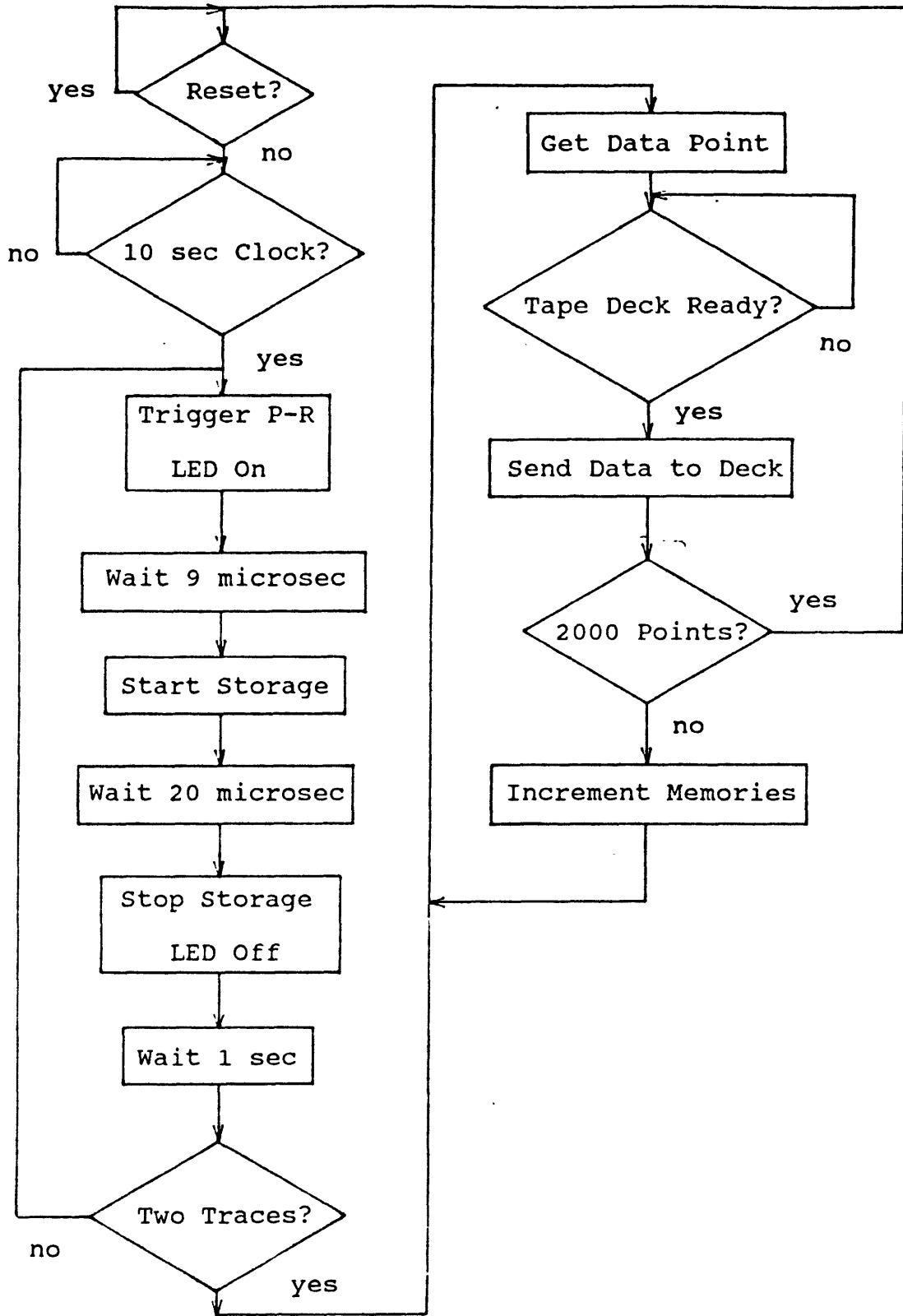
Figure 12: Microprocessor Program Flowchart

2.3 ANALOG SIGNAL ACQUISITION SYSTEM

The analog signal acquisition system provided a completely separate data source for comparison with the digital data. The system consisted of a time syncronized videocamera recording the screen of a high bandwidth (60 Mhz) oscilloscope (see Figure 13). Reduction of the videotape data was accomplished manually. The analog system was connected to an array of 8 transducers mounted around the leading edge of the wing. One of the array transducers was located near the transducer connected to the digital system (same chord position and 7/10 in. spacing spanwise) so that data from the two systems could be compared.
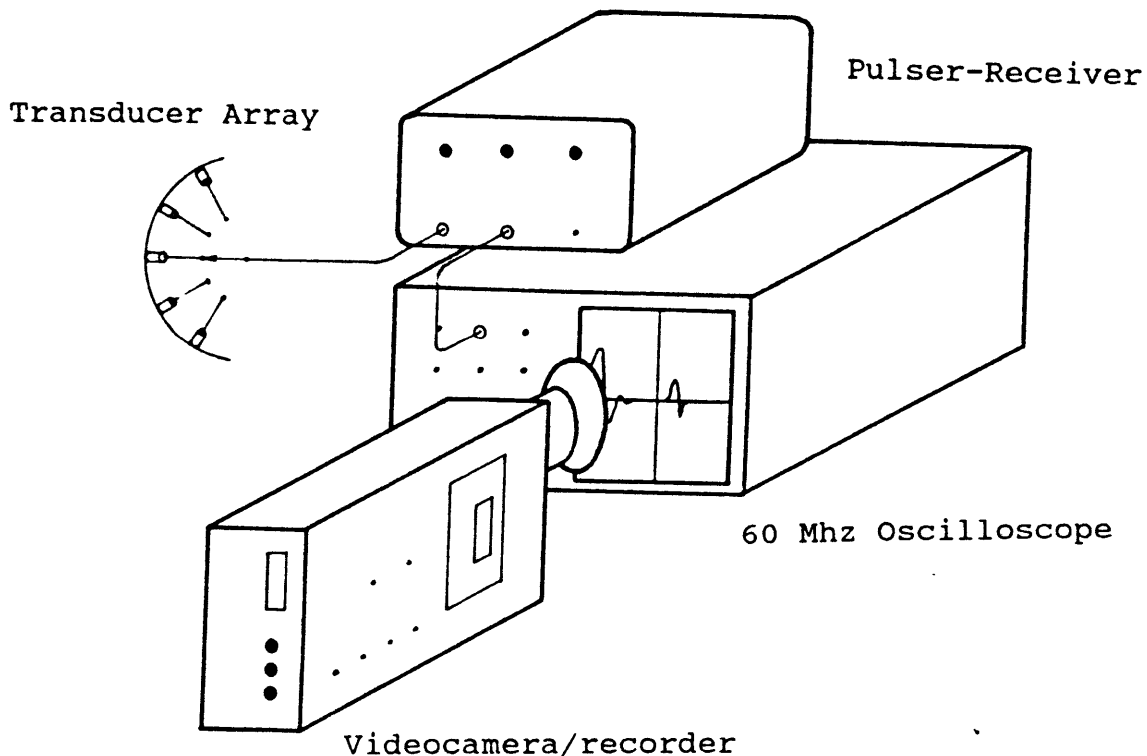
Figure 13: Analog Data Acquisition System

2.4 FLIGHT TEST INSTALLATION

The two signal acquisition systems were installed in NASA's Twin Otter Icing Research Aircraft (shown in Figure 14), based at Lewis Research Center in Cleveland, Ohio. The ultrasonic transducers were mounted in the leading edge of a wing "cuff". The cuff is actually a section of an airfoil mounted over the existing wing as shown in Figure 15. Figure 16 shows the pulser-receiver, digitizer, and tape deck mounted in a rack on the interior of the aircraft. Figure 17 shows the oscilloscope and videocamera.

The test aircraft was equiped to measure several parameters associated with icing clouds. A Johnson-Williams instrument measured liquid water content (LWC) of the cloud; a laser probe measured the droplet size distribution from which the median volume diameter (MVD) of the droplets could be calculated; and thermocouples measured outside air temperature. These parameters were recorded automatically during flight at 10 second intervals.
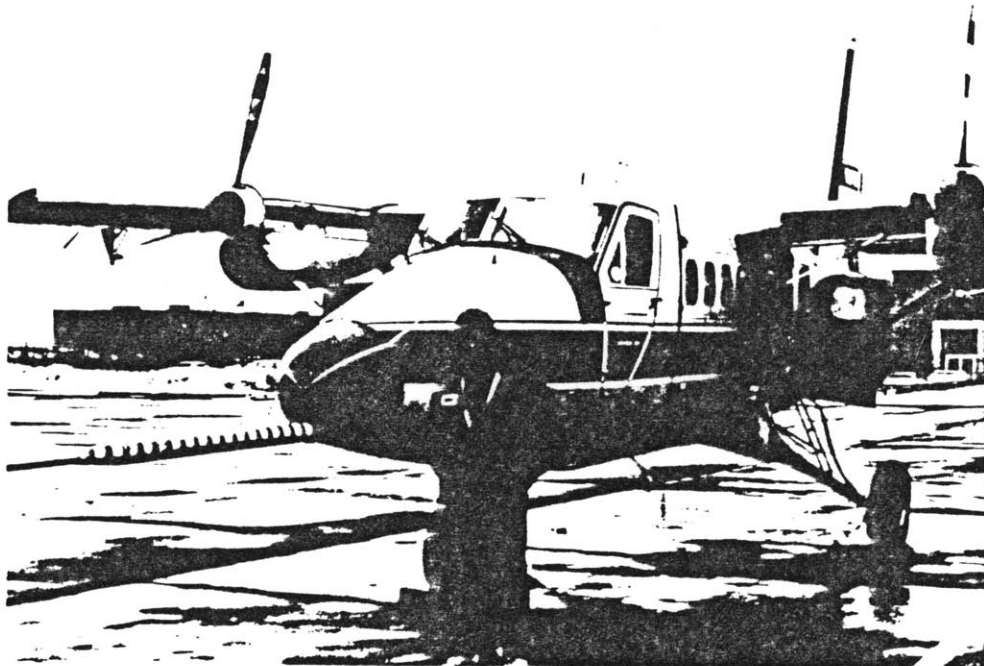
Figure 14: Twin Otter Icing Research Aircraft
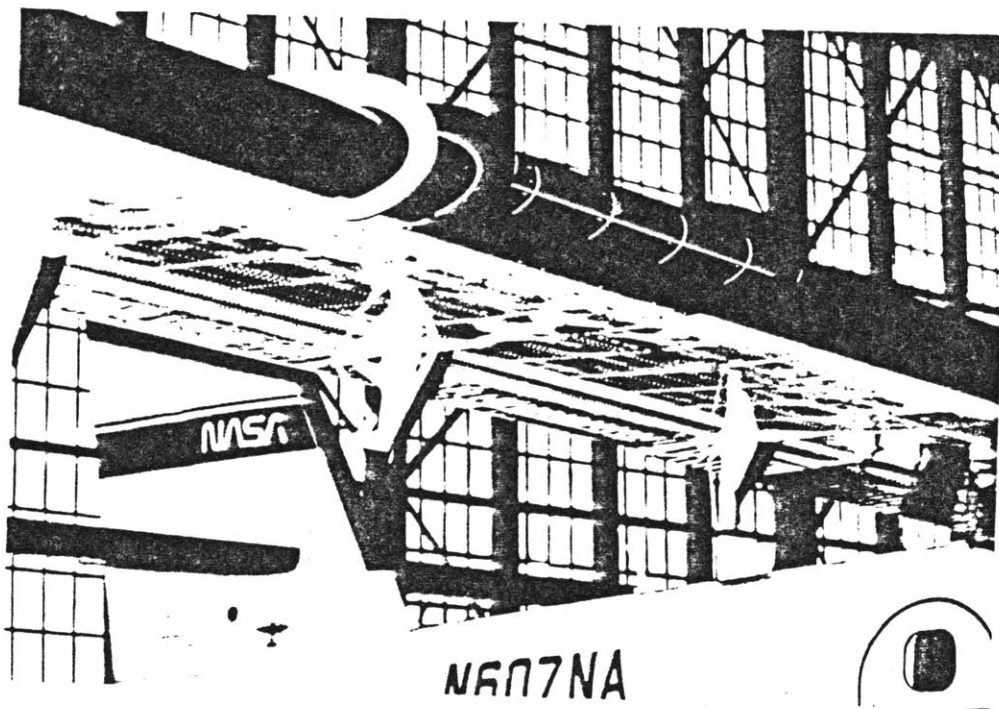
Figure 15: Wing Cuff with Transducers
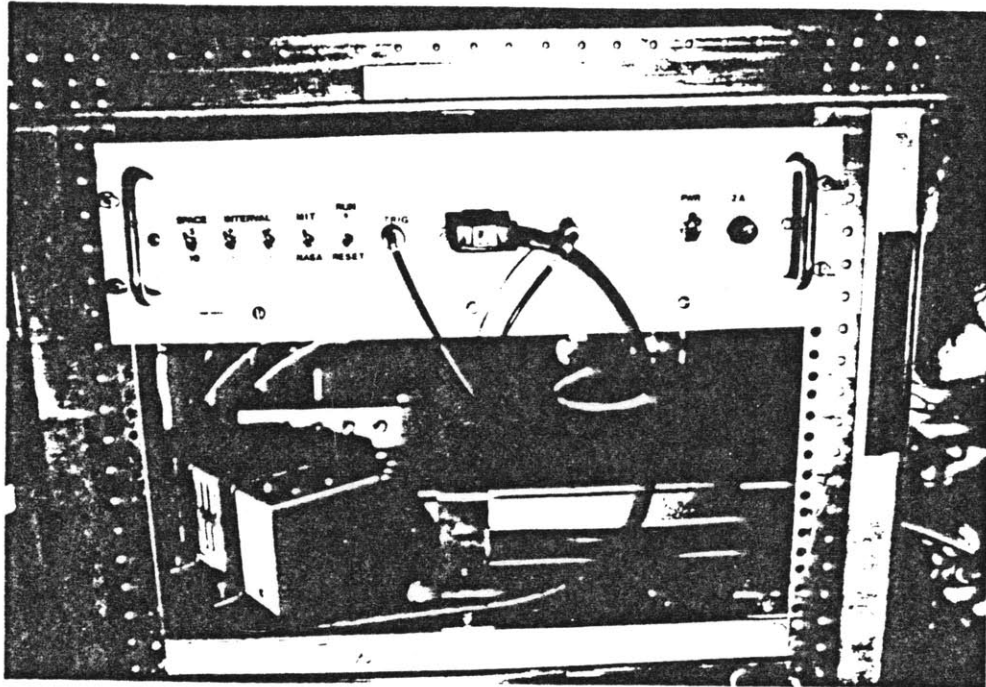
Figure 16:   Data Aquisition System Mounted in Aircraft
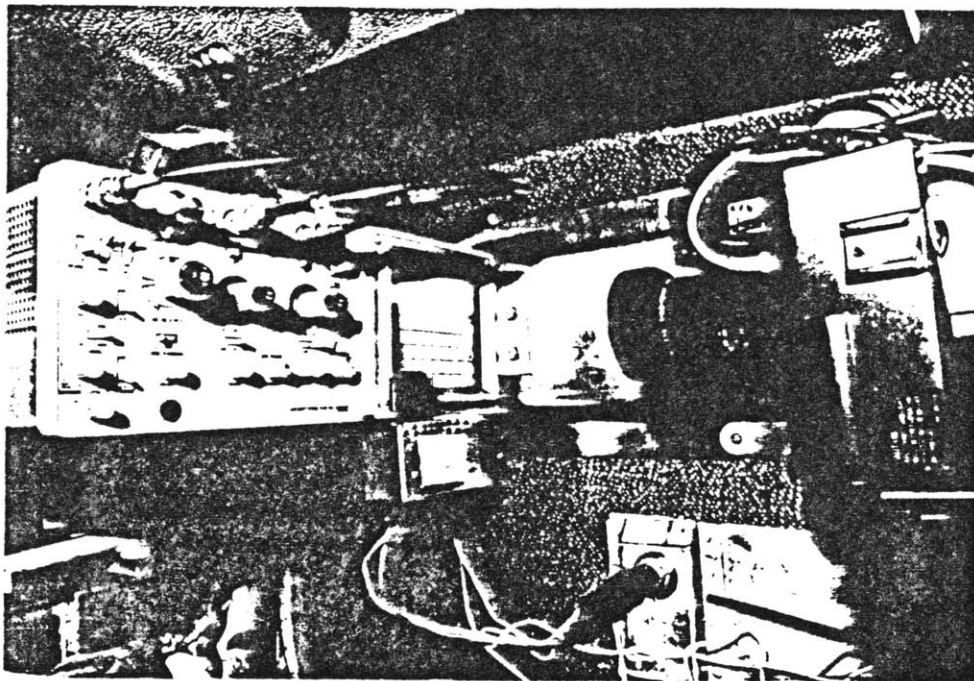
Figure 17:   Oscilloscope and Videocamera

2.5 FLIGHT TEST PROCEDURES

The icing flight tests were conducted at NASA Lewis Research Center in Cleveland, Ohio. The following procedures were used during the tests: At the beginning of the flight, the analog signal aquisition system was started. Shortly after the initiation of icing, the digital signal aquisition system was turned on. Each videotape lasted 90 minutes, enough for an entire flight. The digital tapes, however, could only store about 9 minutes of data per side (see Section 2.1). Therefore, small gaps occurred in the digital data due to tape changes.

The aircraft was flown to areas where icing had been reported and attempted to stay in the icing conditions as long as possible. Because the wing cuff was not de-iced, the ice accretion remained on the cuff until after landing. The ice was then removed and measured with calipers.

3. RESULTS AND DISCUSION

The results of the flight tests and the analysis of the sigal processing algorithms are discused in this chapter. Section 3.1 summarizes the icing conditions encountered and the data acquisition system performance during each flight. Section 3.2 contains examples of the digital signals. The derivative processing used by the algorithms is outlined in Section 3.3. Section 3.4 has descriptions of the thickness algorithms, and plots obtained using them. The digital and analog results are compared in Section 3.5. And finally, Section 3.6 describes the icing rate algorithms.

3.1 FLIGHT SUMMARY

Nine icing flights were conducted between February 6 and March 6, 1986 for this experiment. Three flights, 86-30, 86-31, and 86-32 produced good data for the development of the signal processing algorithms. The icing conditions from these flights are summarized in Table 2. The first two flights, 86-26 and 86-27, were used to establish the proper gain and damping settings. The remaining flights did not produce usable data due to equipment failures (one cable failure and three tape deck malfunctions). A tape deck malfunction also caused two 8 minute data dropouts in flight 86-32. Figures 18, 19, and 20 show the ice formations on the wing cuff for the three successful flights. The icing conditions encountered

during the three flights did not vary much. All three
conditions produced slow dry growths.

Table 2: Flight Data Summary

FLIGHT	86-30	86-31	86-32
Date	26FEB86	26FEB86	4MAR86
Temp (°C)	-8.5	-10.0	-6.0
LWC (gm/m^3)	0.10	0.10	0.20
MVD (microns)	N/A	22.0	15.0
Ice Thickness (mm)	7.8	8.6	10.2
Exposure Time (min)	65	55	60

Notes: Static temperature is shown. LWC is the liquid
water content of the cloud measured using a
Johnson-Williams hot-wire probe. MVD is the
median volume diameter of the droplets calculated
from laser-probe measurements of the droplet size
distribution (not available for 86-30). The ice
thickness shown is the mechanical measurement
taken after landing.
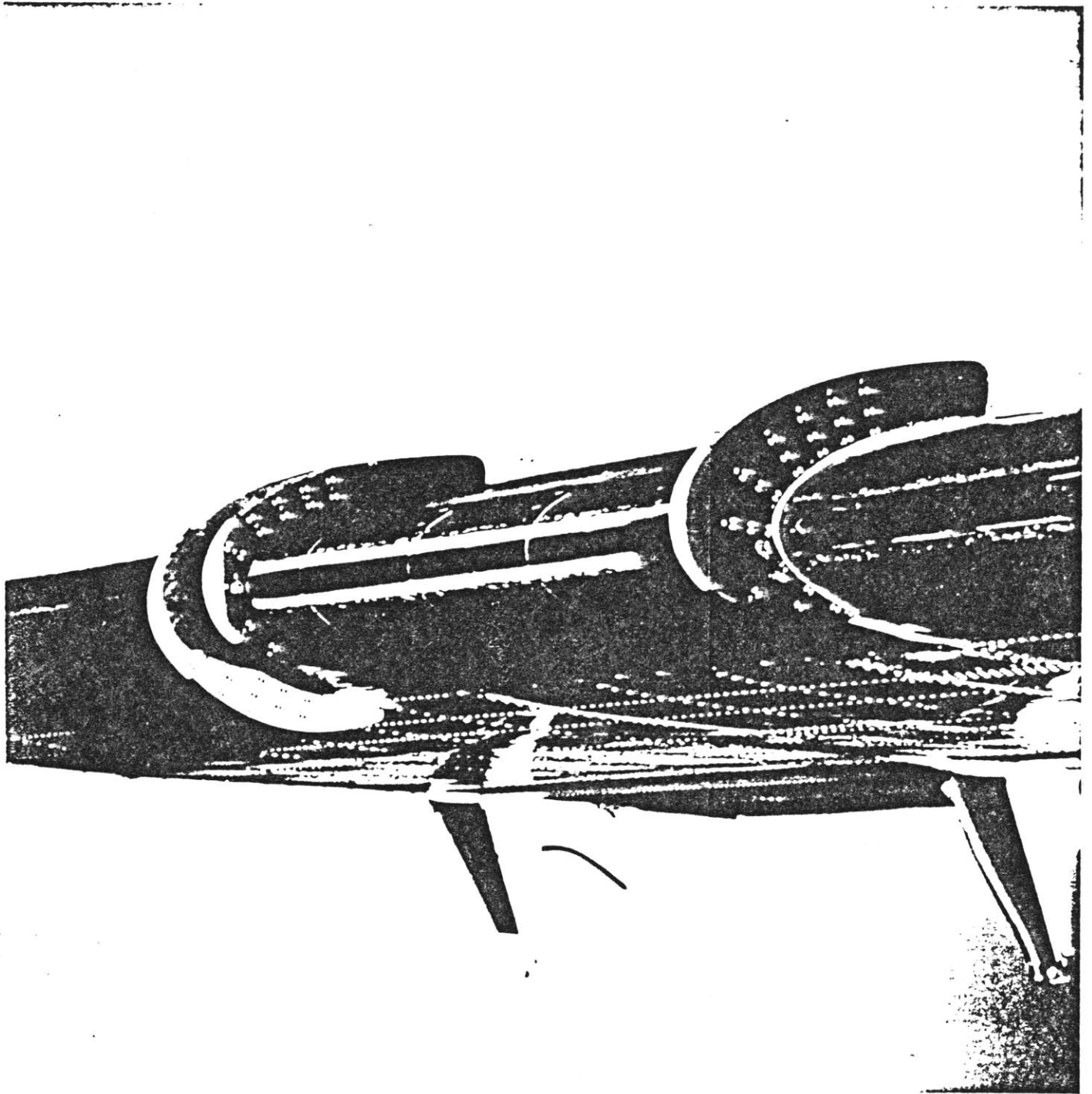
Figure 18: Ice Formation for Flight 86-30
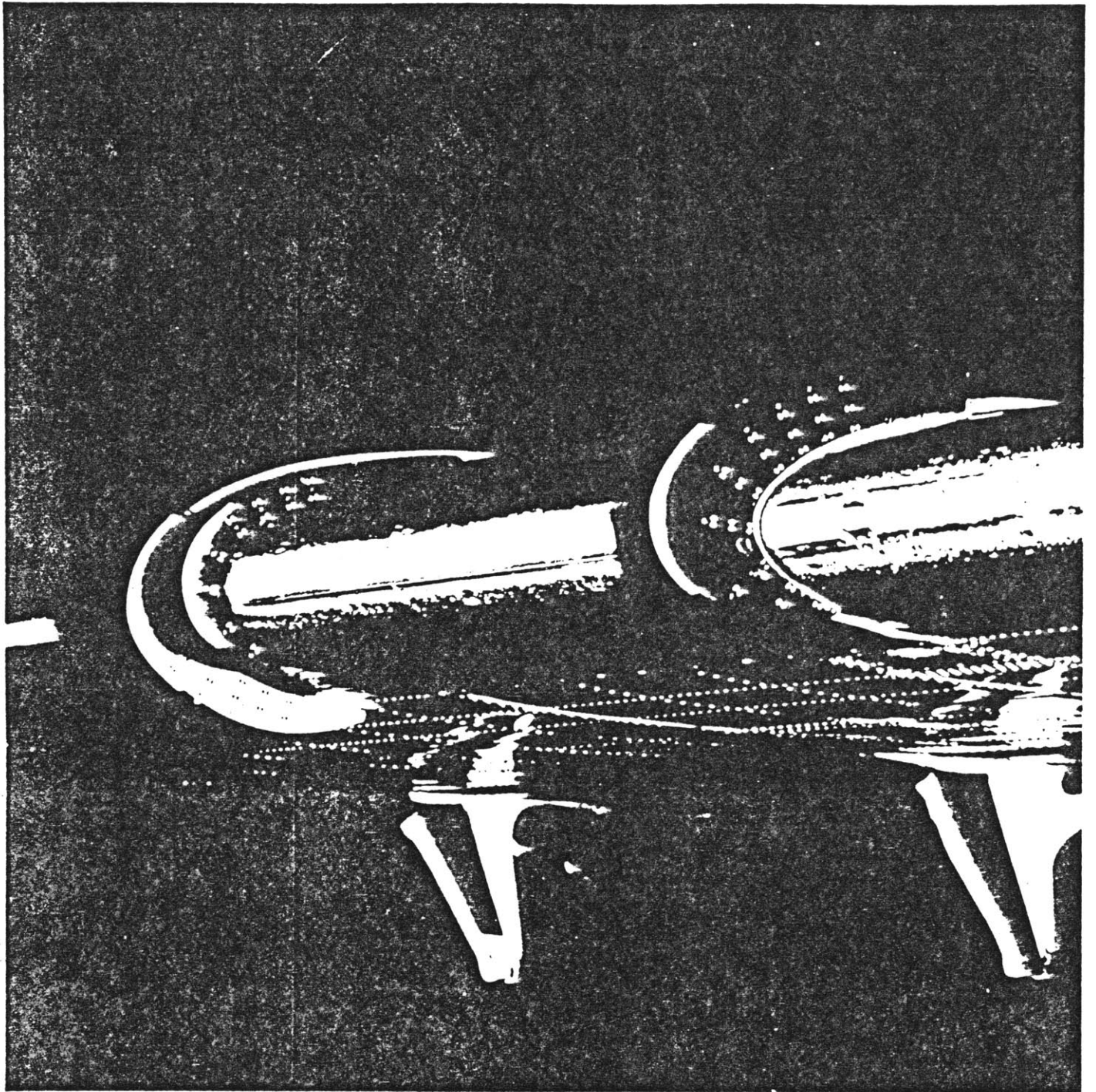
Figure 19:   Ice Formation for Flight 86-31
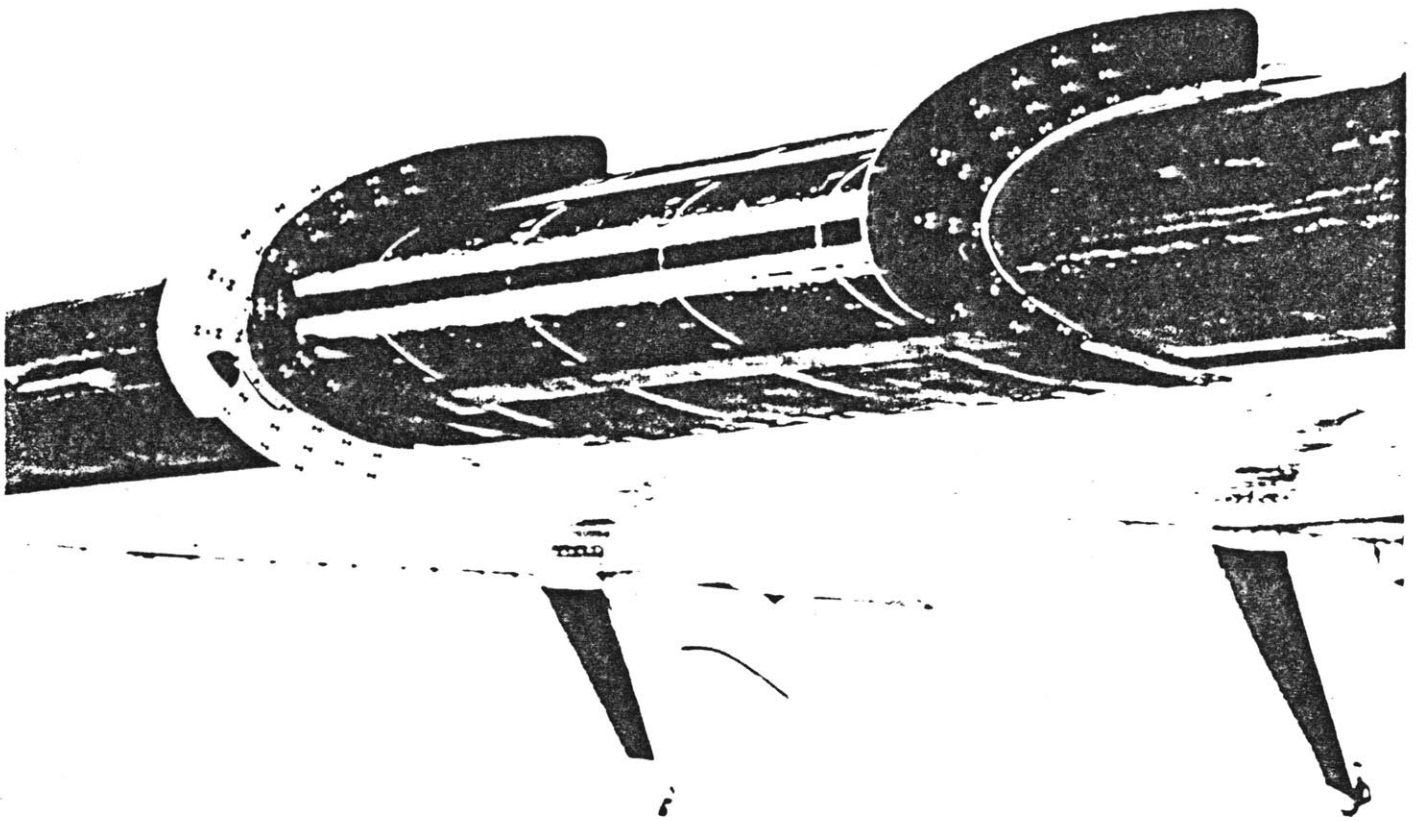
Figure 20: Ice Formation for Flight 86-32

3.2 DIGITAL SIGNAL EXAMPLES

Before describing the algorithms, it is useful to examine example waveforms stored by the digital system. The following figures are examples of waveforms encountered during the flight tests. Figure 21 shows a typical waveform with a clean echo, from which the pulse-echo time is easily determined. Note that the first sample point occurs 9 microseconds after the trigger, so that the plexiglass/ice echo occurs 1 microsecond later, at the 50th sample point. Since the samples were taken at a fixed rate (20 nanoseconds between samples or 50 sample intervals per microsecond), the number of sample intervals between any two sample points determines the elapsed time. The number of sample intervals between the ice/air echo point and the 50th point corresponds to the pulse-echo time:

$$T_{p-e} = ((\text{ice/air point \#}) - 50)/50 \tag{2}$$

Where T_{p-e} is in microseconds. For example, the ice/air point in Figure 21 was the 260th sample so that $T_{p-e} = (260-50)/50 = 4.2$ microseconds. Using equation (1):

$$D = C \cdot T_{p-e}/2 \tag{1}$$

The ice thickness for the waveform in Figure 21 then is D = (3.8mm/microsec)(4.2 microsec)/2 = 7.98 millimeters.
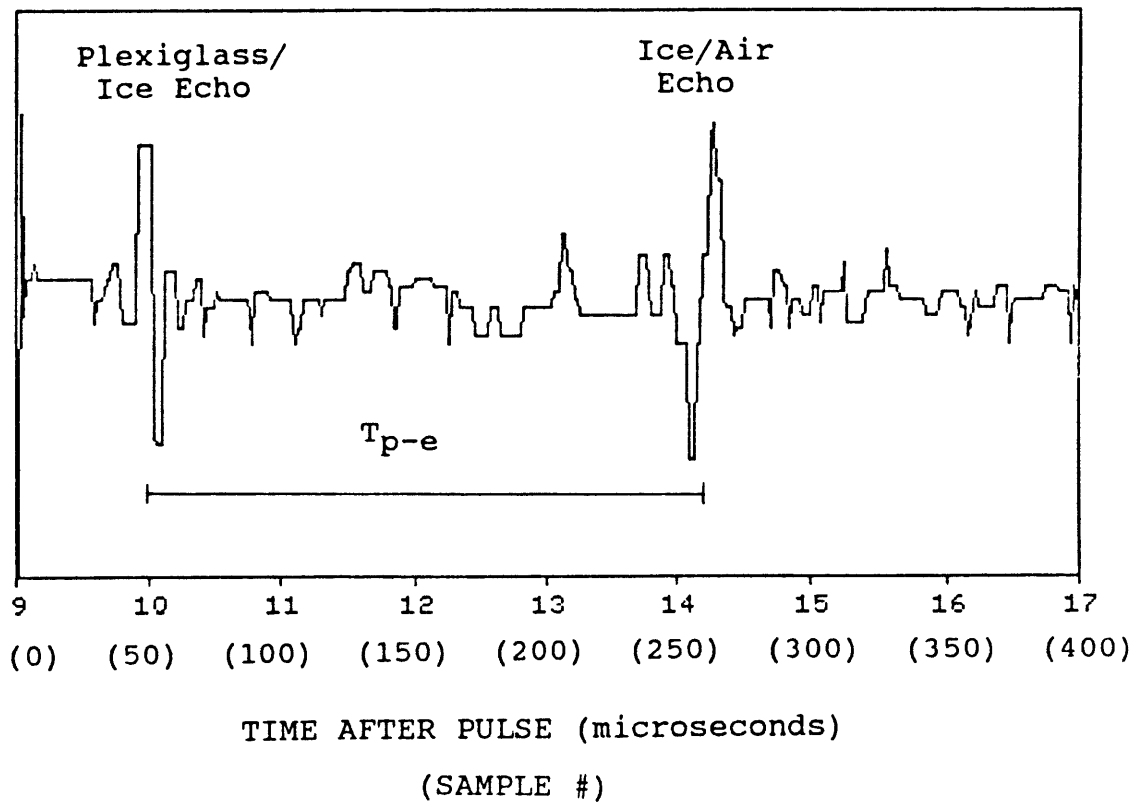
Figure 21: Typical Digitally Stored Waveform

Figures 22 through 24 show the effects of the gain and
damping settings on the pulser-receiver. With the gain
too high (shown in Figure 22), the echo magnitude and some
of the noise peaks are out of the dynamic range of the
digitizer, and they cannot be differentiated from one
another. With the gain too low (shown in Figure 23), the
echo magnitude is in the noise level. Insufficient
damping (shown in Figure 24) causes an excessive pulse
width (compare the plexiglass/ice interface widths in
Figures 21 and 24).

TIME AFTER PULSE (microseconds)
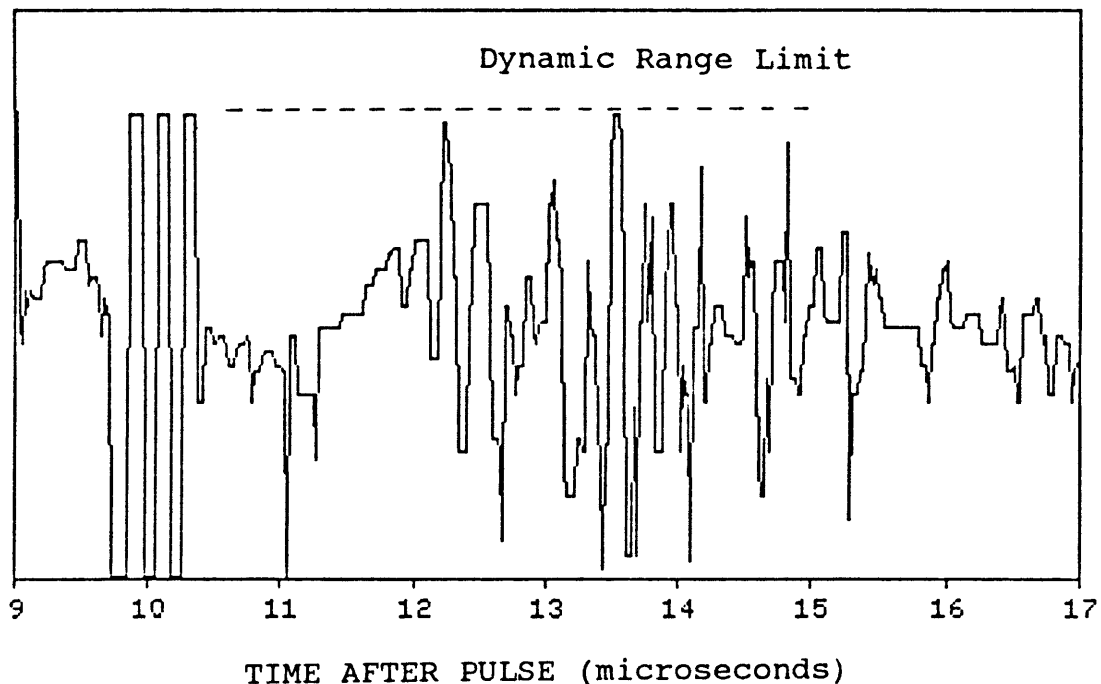
Figure 22: Digital Waveform with Pulser-Receiver
Gain Too High
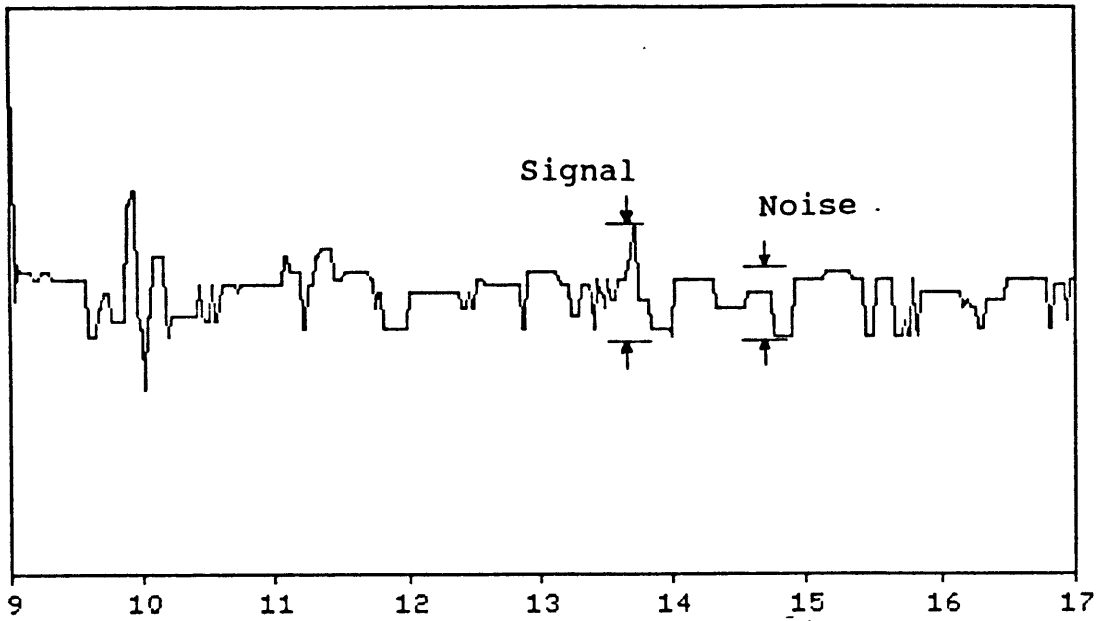
Figure 23: Digital Waveform with Pulser-Receiver
Gain Too Low
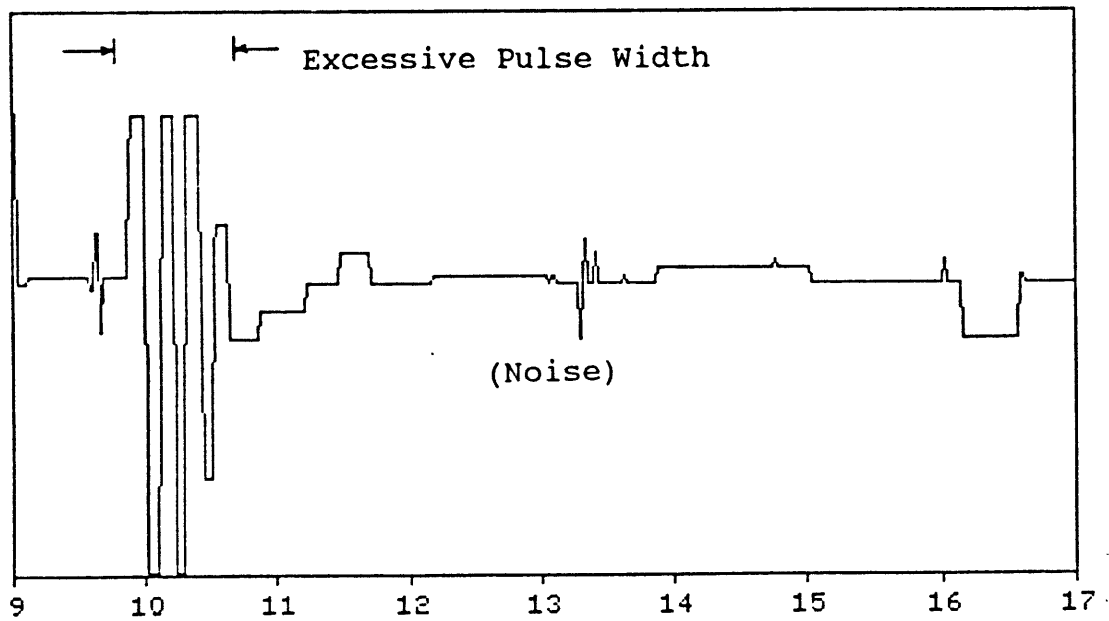
Figure 24: Digital Waveform with Pulser-Receiver
Damping Too Low

Figures 25 and 26 show the effect of a layer discontinuity in the ice, which can occur from an abrupt change in the icing conditions or from a layer of snow trapped in the ice. When the ice/air interface is near the layer, the echo from it is generally greater than the layer echo. However, as the ice gets thicker, the ice/air echo experiences increased attenuation due to the increased path length and may become lower in amplitude than the earlier layer echo.

Plexiglass/Ice Echo

TIME AFTER PULSE (microseconds)
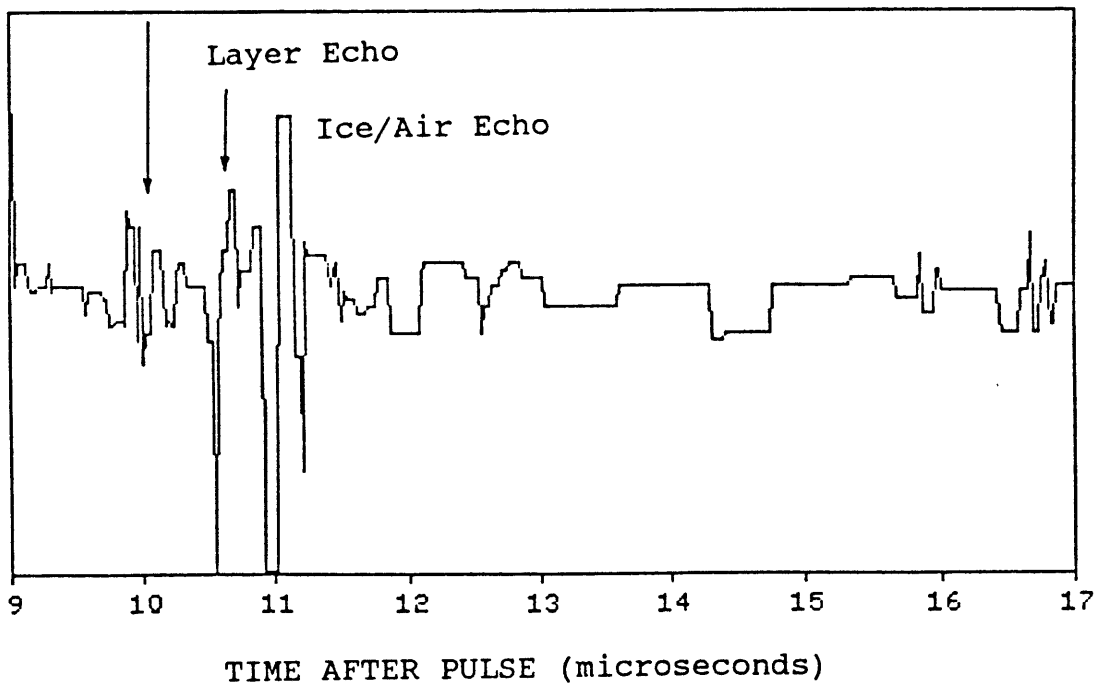
Figure 25: Digital Waveform from Layered Ice

with Ice/Air Interface Near Layer
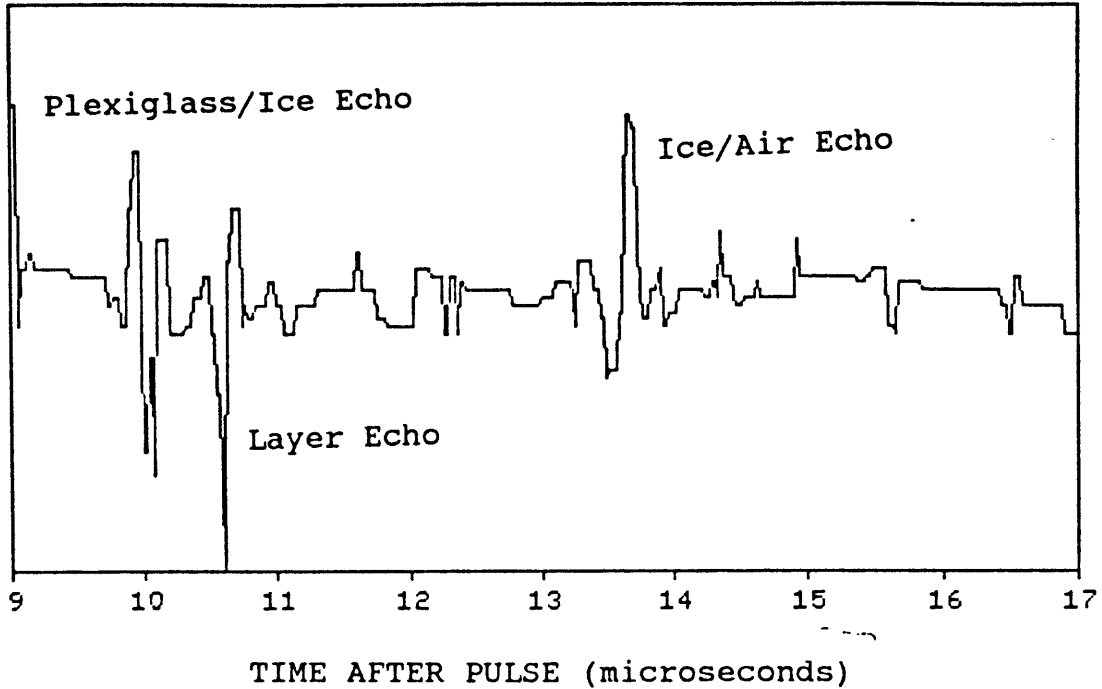
Figure 26: Digital Waveform from Layered Ice
with Ice/Air Interface Far from Layer

3.3   DERIVATIVE PROCESSING

The thickness algorithms described in the next section
attempt to determine which sample point corresponds to the
center of the ice/air echo. One method of selecting a
consistent point within the echo is to compute the
derivative of the waveform. A peak in the magnitude of
the derivative usually corresponds to the center of the
echo. Figures 27 and 28 show typical waveforms and the
magnitudes of their derivatives. All of the thickness
algorithms described in the next section preprocess the
waveforms using a 5-point descrete approximation to the
derivative.
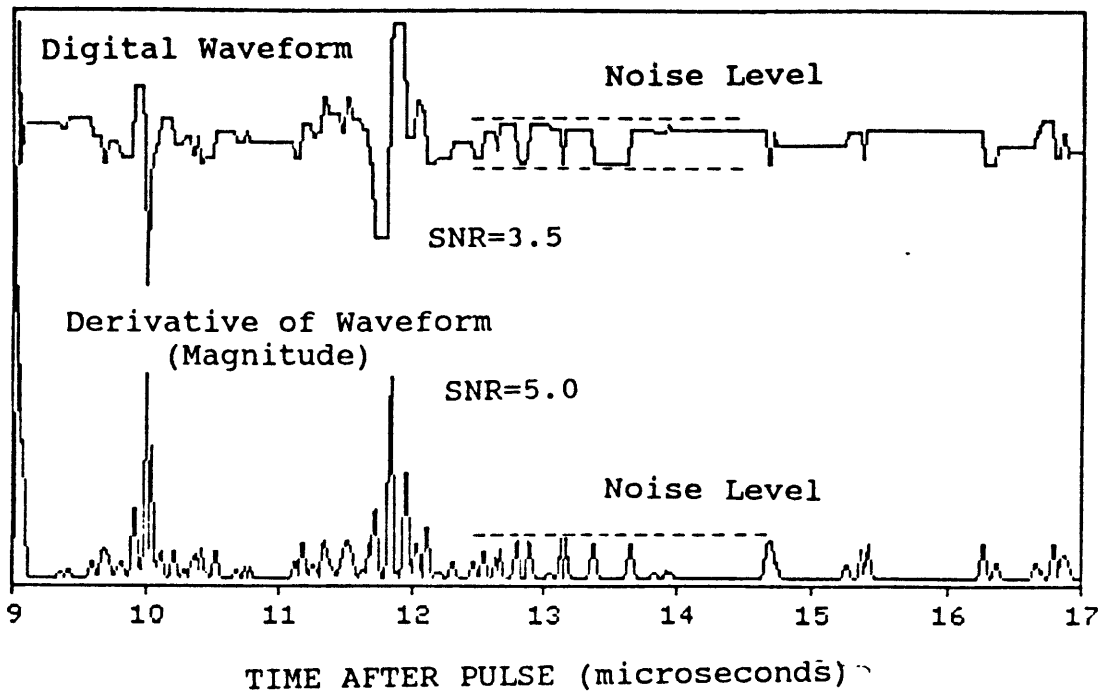
Figure 27: Derivative of Digital Waveform

5-Point Approximation
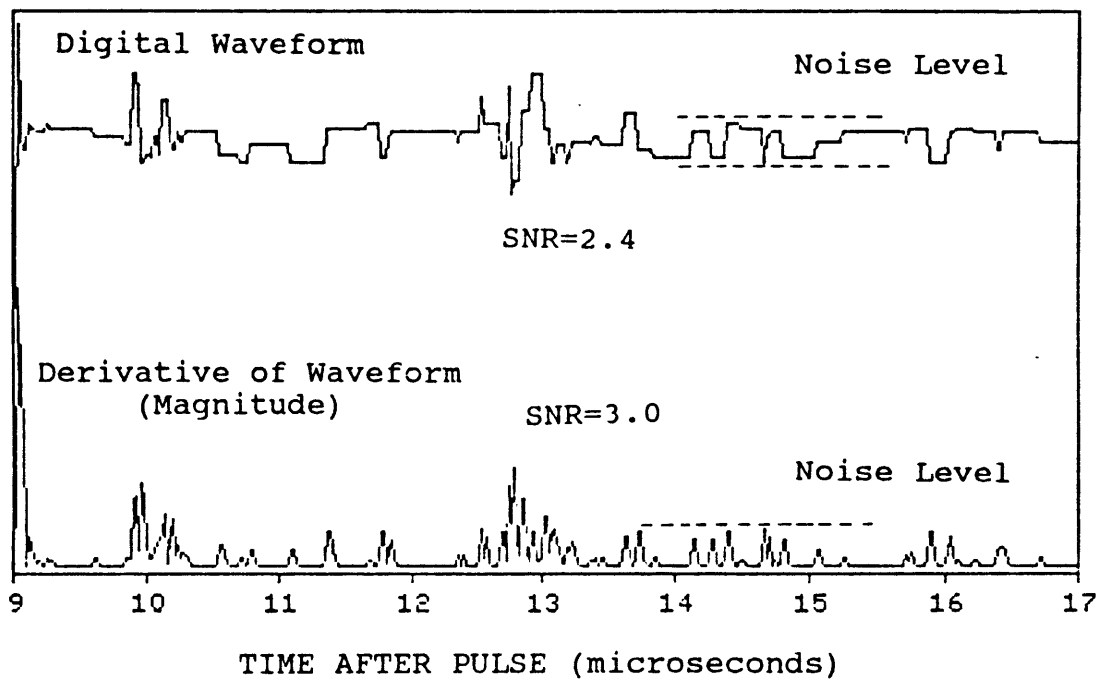
Figure 28: Derivative of Digital Waveform

5-Point Approximation

The following formula gives the 5-point apprximation to the derivative:

$$(d/dt)U_t = (1/12)U_{t-2}-(2/3)U_{t-1}+(0)U_t+(2/3)U_{t+1}-(1/12)U_{t+2} \quad (3)$$

Where U_t is the sample of signal U at time t. This approximation gives the proper derivative for linear, quadradic, and cubic functions of U (the coefficeints were derived by substituting U, U^2, U^3, and their derivatives into the equation and solving the resulting system of equations). Approximations with less than 5-points did not work very well, while approximations with more than 5-points did not provide enough added improvement to justify the added computation time. In addition to selecting a consistent echo point, derivative processing improves the signal to noise ratio. The peak in the magnitude of the derivative has a greater SNR than the peak in the magnitude of the original waveform (as shown in Figures 27 and 28).

Figures 27 and 28 also illustrate the system noise level. The noise levels shown in the figures were consistantly observed throughout the flights. This noise was most likely from the pulser-receiver and the digitizer. The signal to noise ratio of the ultrasound itself was probably much better.

3.4 THICKNESS ALGORITHMS

Four thickness algorithms are presented in this section, in order of increasing complexity. Each algorithm attempts to determine which sample point in the waveform corresponds to the ice/air echo and then uses Equation (2) to determine the pulse-echo time and Equation (1) to determine the ice thickness. Table 3 summarizes the methods employed by each algorithm for determining the ice/air echo point. The results from each algorithm are presented immediately following its description to provide motivation for the succeeding algorithms. Conclusions about the algorithms are summarized in Chapter 4.

Table 3: Algorithm Summary

Algorithm 1 - Peak detector with derivative preprocessing.

Algorithm 2 - Peak detector with derivative preprocessing and low SNR filtering.

Algorithm 3 - Gated peak detector with derivative preprocesssing and low SNR filtering.

Algorithm 4 - Gated peak detector with derivative preprocessing, low SNR filtering, and two measurement averaging.

Algorithm 1 is a simple peak detector. It first computes the derivative of the waveform, and then chooses the largest peak. It ignores the first 1.4 microseconds of data (70 points), where the plexiglass/air echo occurs, resuting in a minimum detectable ice thickness of 0.76 millimeters. Figures 29a, 30a, and 31a show the thickness of the ice versus time derived using Algorithm 1 for the three flights. Figures 29b, 30b, and 31b show the SNR versus time, which is the ratio between the peak selected and the average noise level (see the discussion at the end of Section 3.3).

The data gaps apparent in the figures are from changing the data tapes (each tape held about 9 minutes of data). The two 8 minute gaps in the data from flight 86-32 (Figure 31) are from tape deck malfunctions.
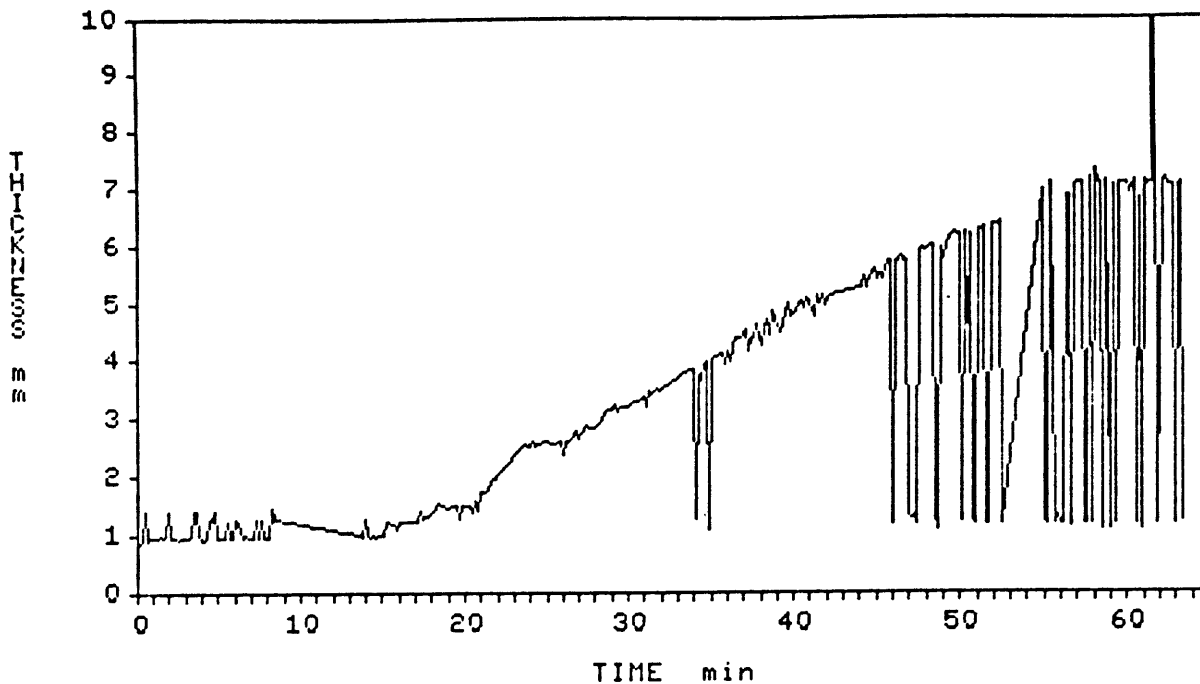
Figure 29a: Ice Thickness vs. Time

Flight 86-30 Using Algorithm 1
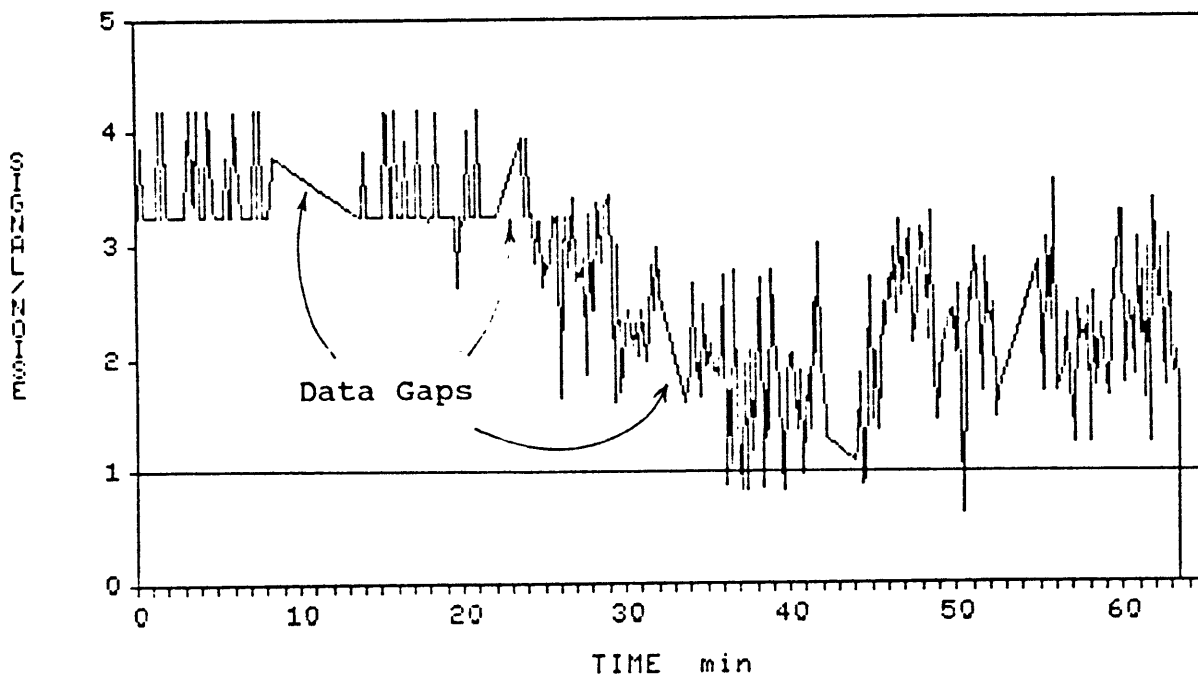
Figure 29b: Signal to Noise Ratio vs. Time

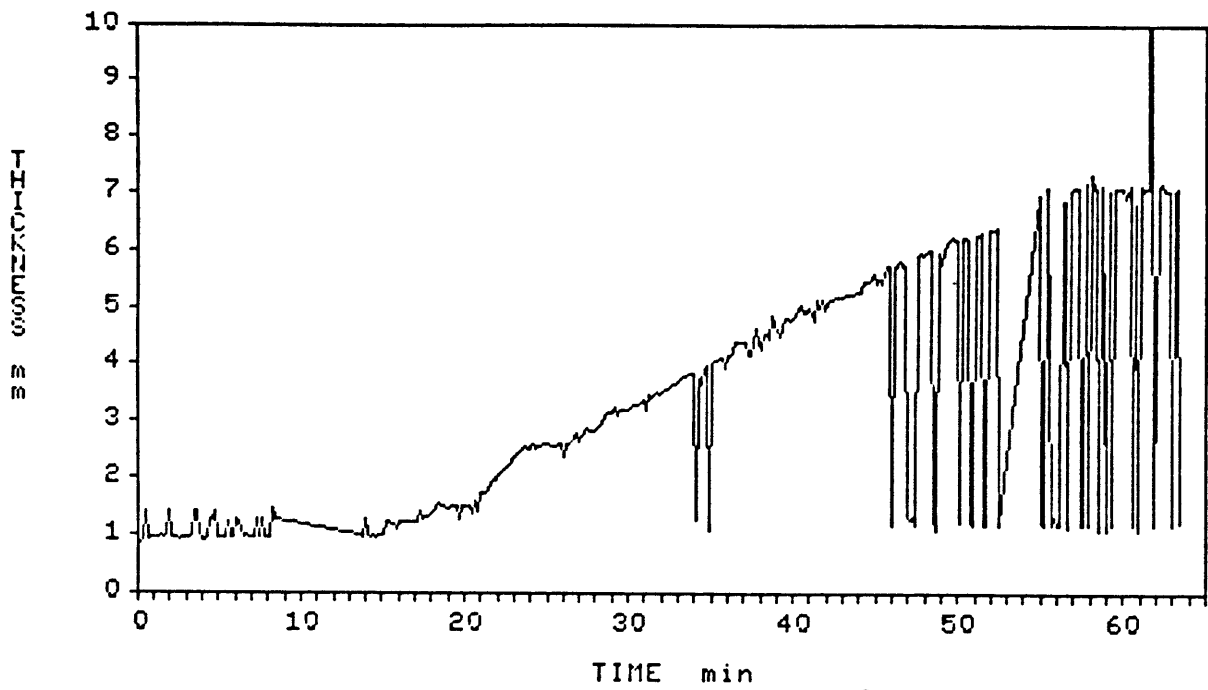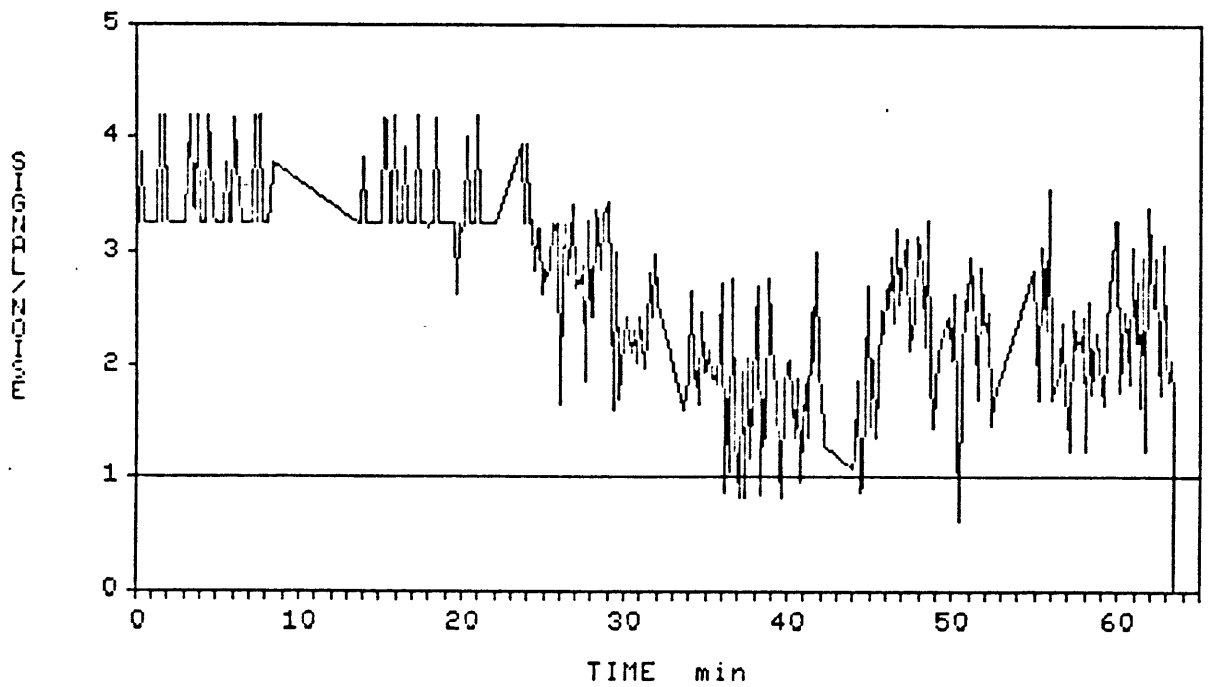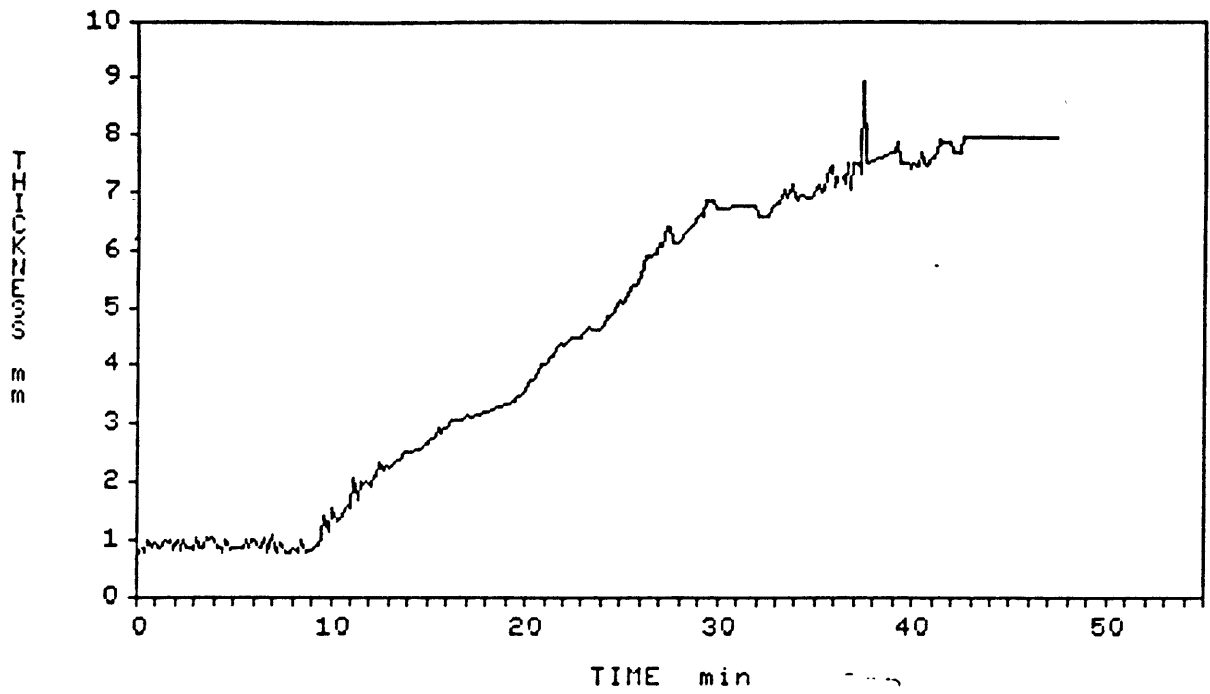Flight 86-30 Using Algorithm 1

-49-
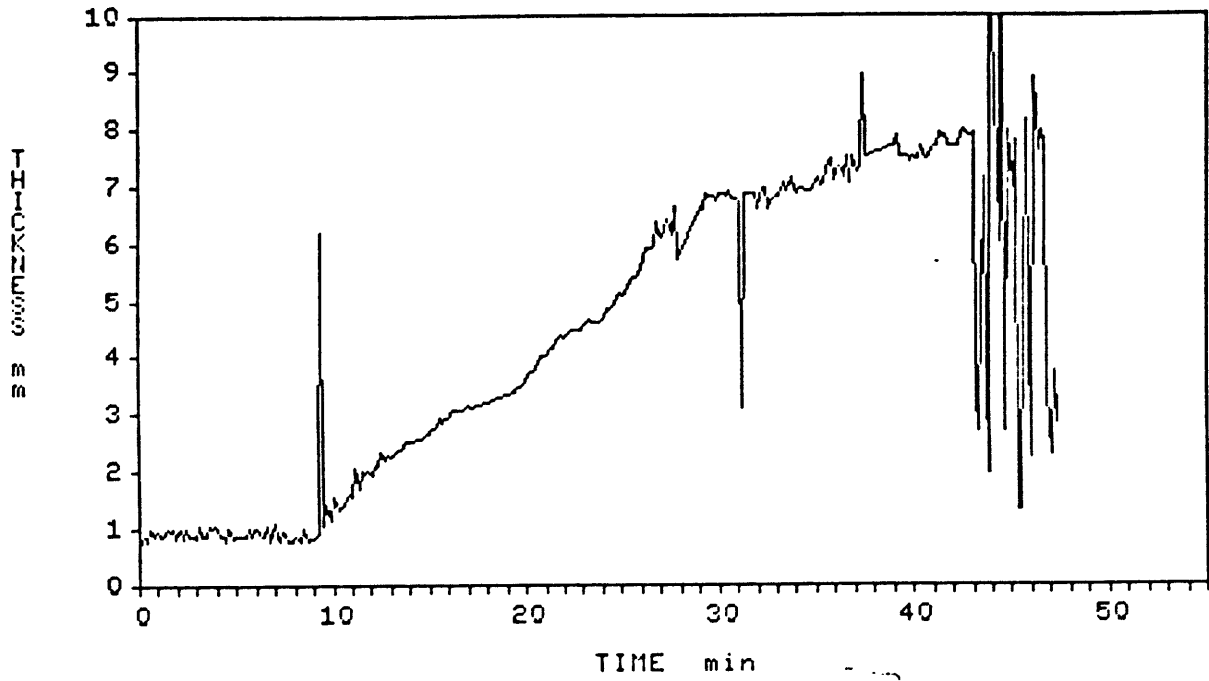
Figure 30a: Ice Thickness vs. Time
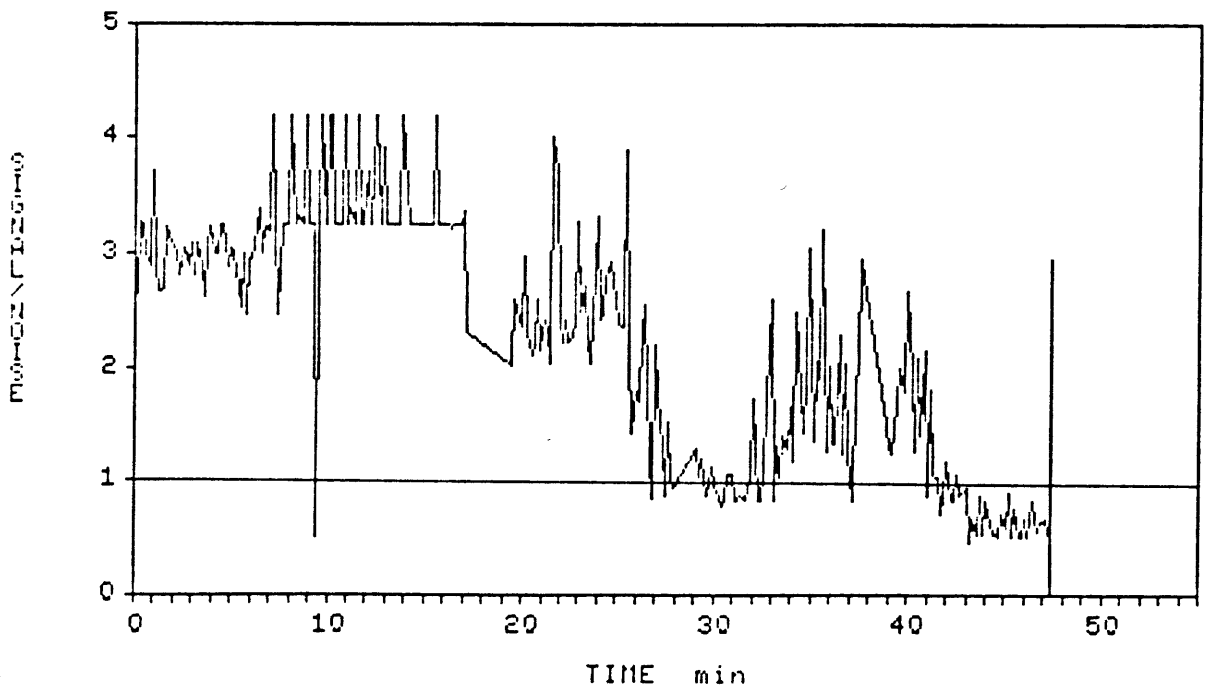
Flight 86-31 Using Algorithm 1
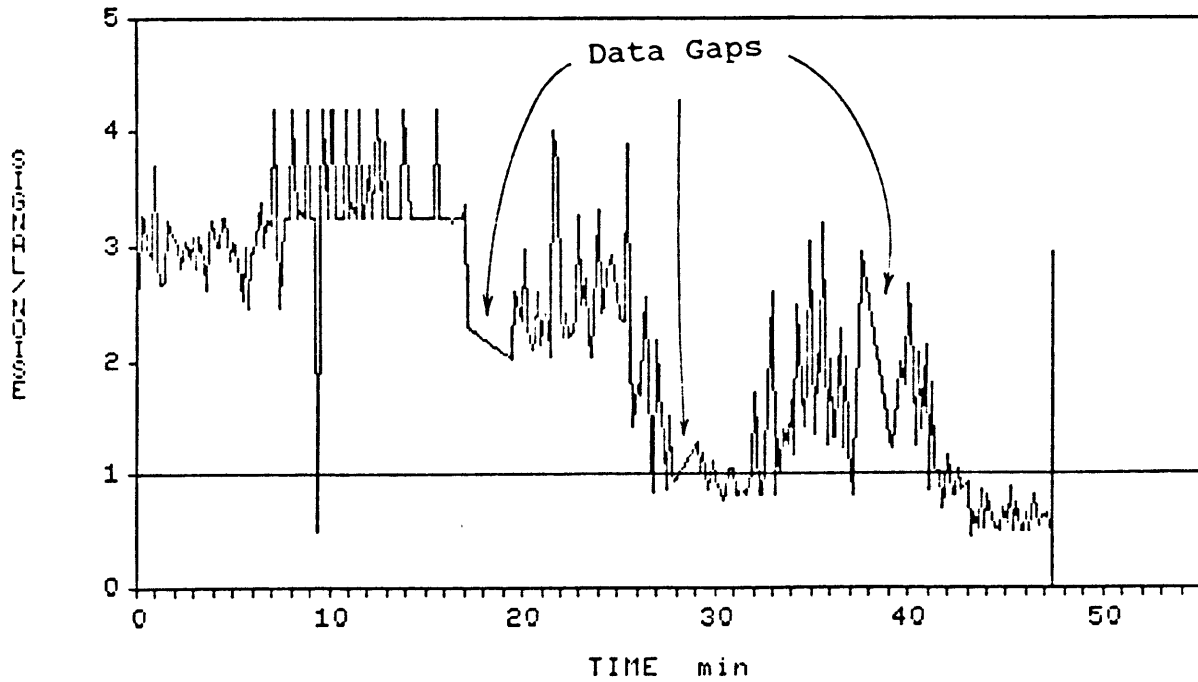
Figure 30b: Signal to Noise Ratio vs. Time

Flight 86-31 Using Algorithm 1
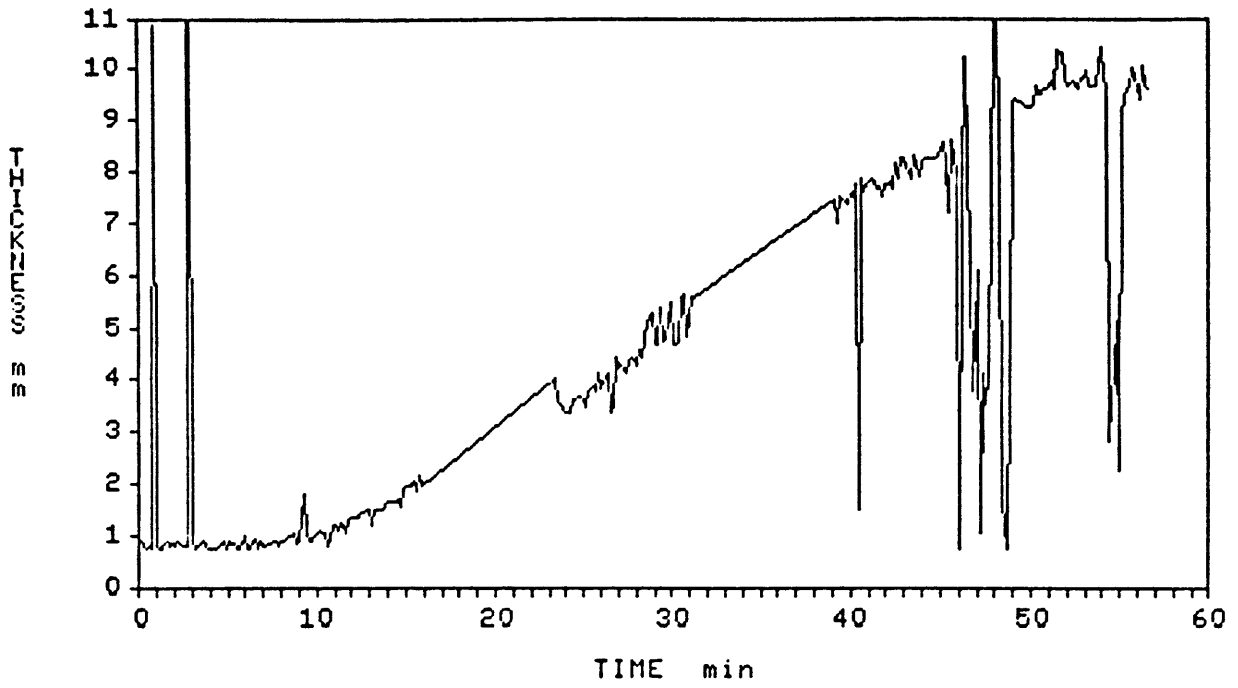
Figure 31a: Ice Thickness vs. Time

Flight 86-32 Using Algorithm 1
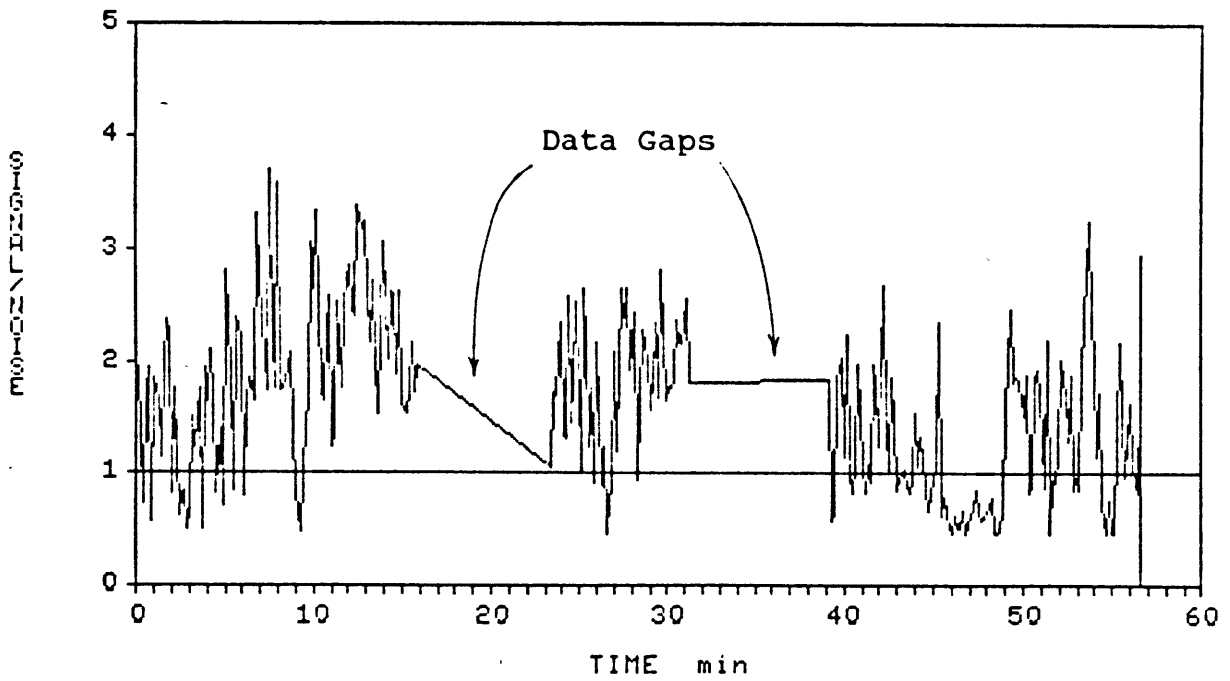
Figure 31b: Signal to Noise Ratio vs. Time

Flight 86-32 Using Algorithm 1

Figure 29 shows that Algorithm 1, the simple peak detector, sometimes vascillates between two ice thickness values. This problem is solved by Algorithm 3, and will be discussed later. First, examination of Figures 30 and 31 reveal that Algorithm 1 outputs random thicknesses when the SNR is close to 1 (it chooses a random noise peak rather than the ice/air echo peak). Algorithm 2 eliminates this problem by discarding any thickness measurements where the SNR is below 1. It replaces these measurements with the previously measured thickness. Figures 32, 33 and 34 show the ice thickness and SNR plots for the three test flights using Algorithm 2.

Figure 32a: Ice Thickness vs. Time

Flight 86-30 Using Algorithm 2

Figure 32b: Signal to Noise Ratio vs. Time

Flight 86-30 Using Algorithm 2

Figure 33a: Ice Thickness vs. Time

Flight 86-31 Using Algorithm 2

Figure 33b: Signal to Noise Ratio vs. Time
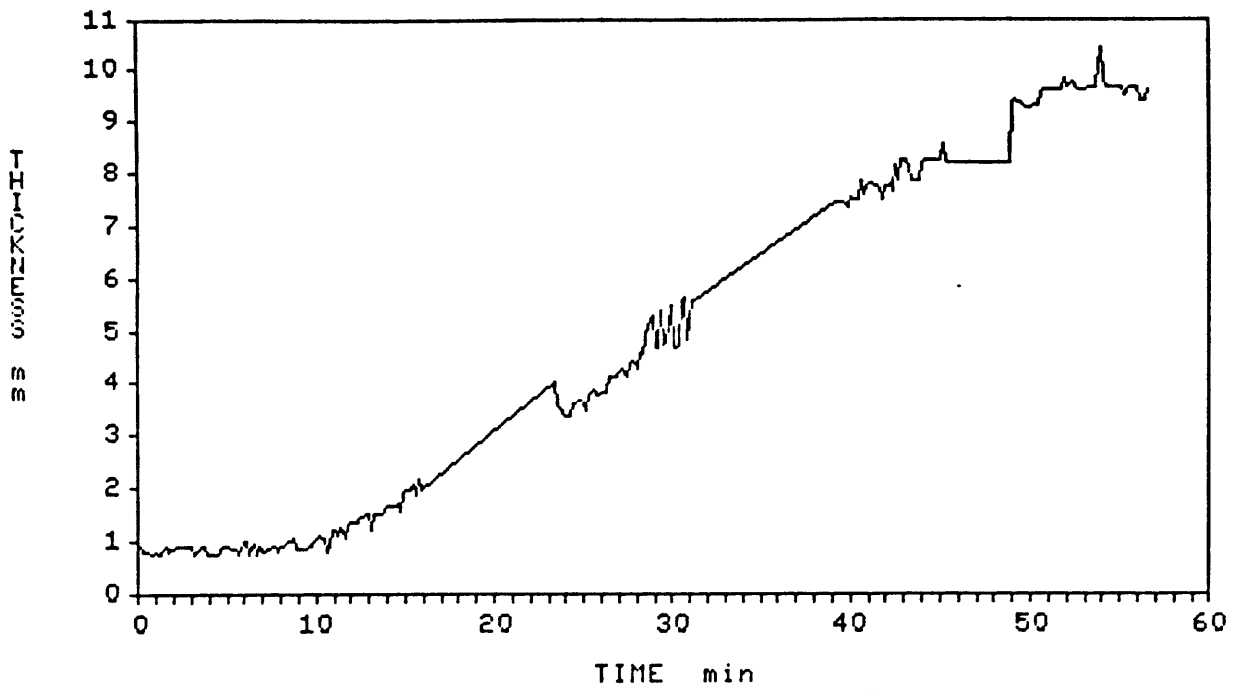
Flight 86-31 Using Algorithm 2

Figure 34a: Ice Thickness vs. Time
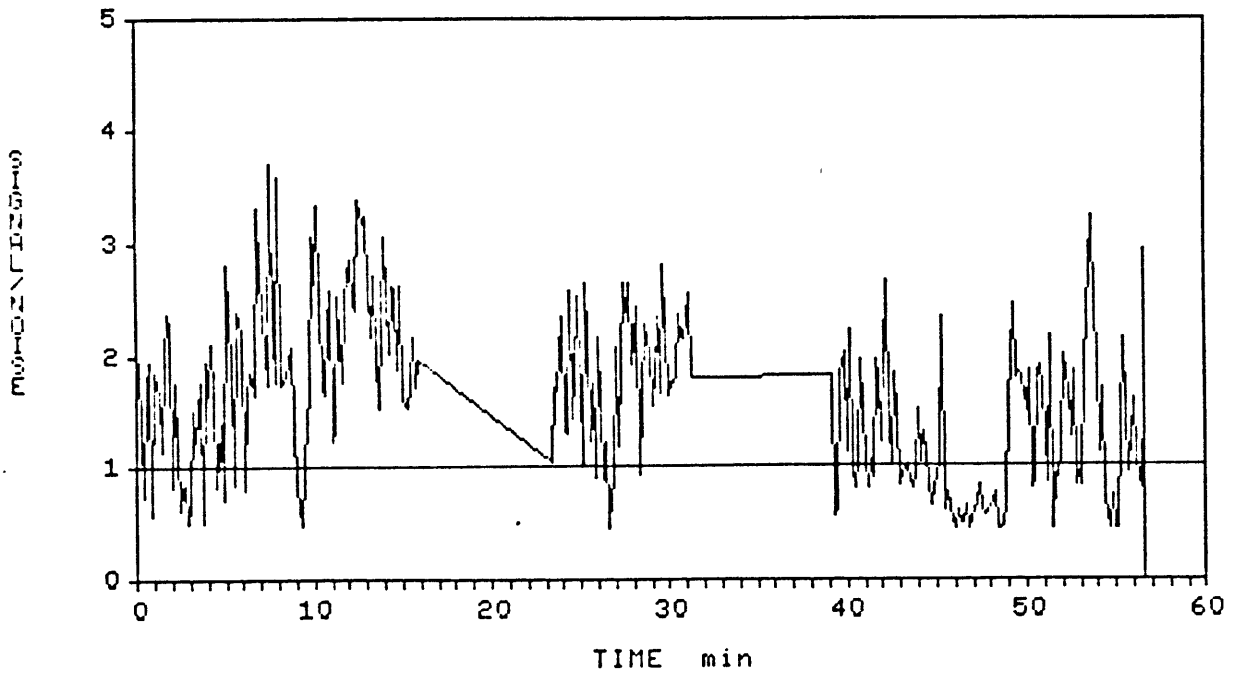
Flight 86-32 Using Algorithm 2

Figure 34b: Signal to Noise Ratio vs. Time

Flight 86-32 Using Algorithm 2

Algorithm 2, with low SNR filtering, worked better
than Algorithm 1 on flights 86-31 and 86-32, but the
vascilation between two values is still apparent in
the results from 86-30 (Figure 32). Examination of the
waveforms from flight 86-30 reveal an echo from a layer as
shown earlier in Figures 25 and 26. When the ice is thick,
Algorithms 1 and 2 sometimes choose the layer echo rather
than the ice/air echo.

Algorithm 3 is a gated peak detector designed to
ignore layer echos or any other noise between the pulse
and the echo. Algorithm 3 looks for the peak in the
derivative within a 1 microsecond wide gate. The gate is
initially set from 1.4 to 2.4 microseconds. As the ice
grows the gate is moved to track the position of the
ice/air echo. The gate begins 0.3 microseconds (15
points) before the previously measured ice/air echo and
ends 0.7 microseconds (35 points) after it. Any noise or
layer echos occuring before or after the gate are ignored.
As with Algorithm 2, Algorithm 3 throws out measurements
with SNR's below 1. Figures 35, 36, and 37 are the
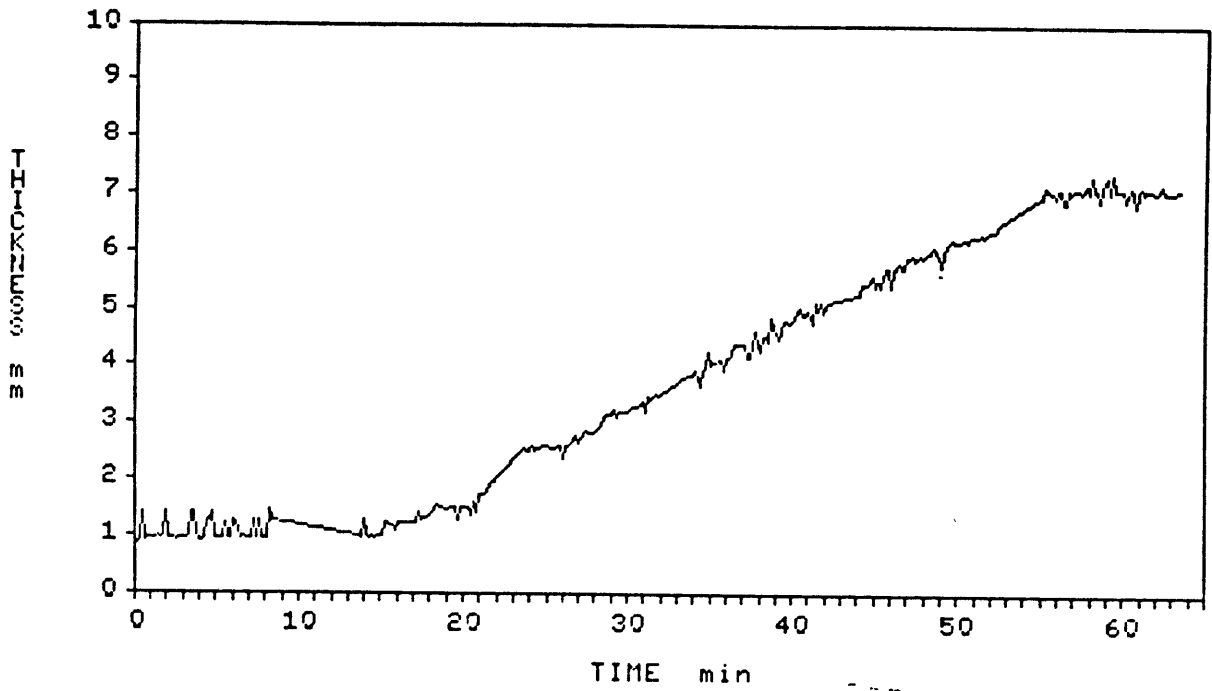thickness plots obtained with Algorithm 3.

Figure 35: Ice Thickness vs. Time

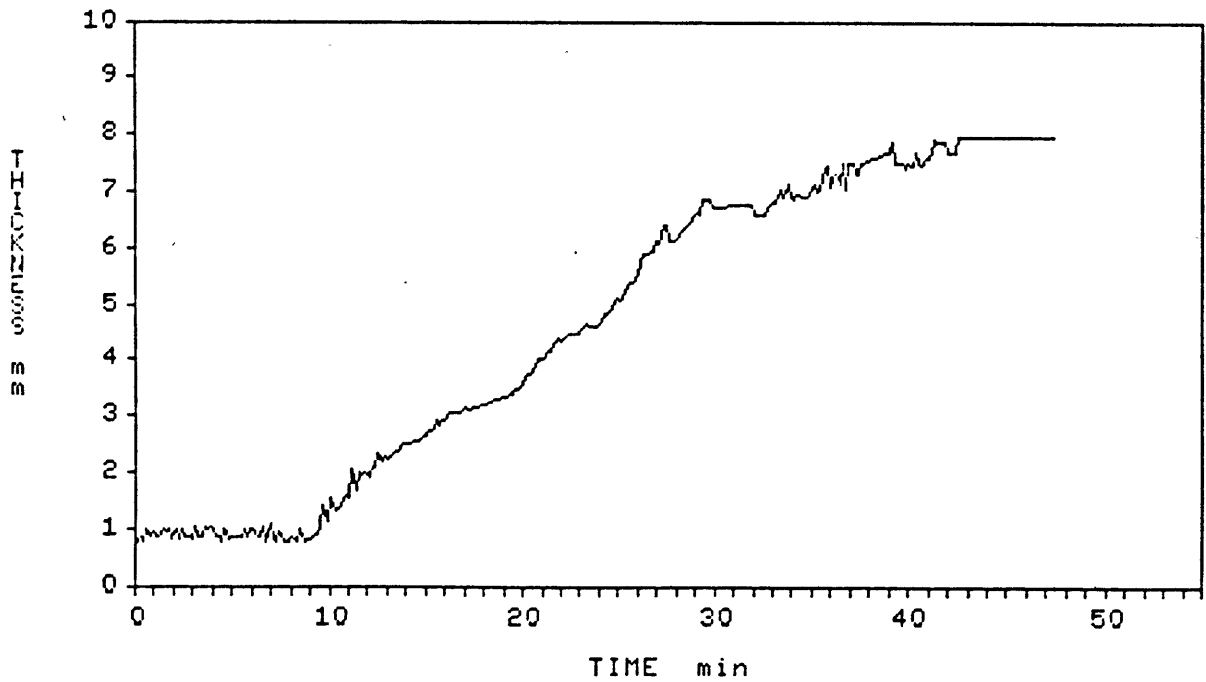**Flight 86-30 Using Algorithm 3**

Figure 36: Ice Thickness vs. Time
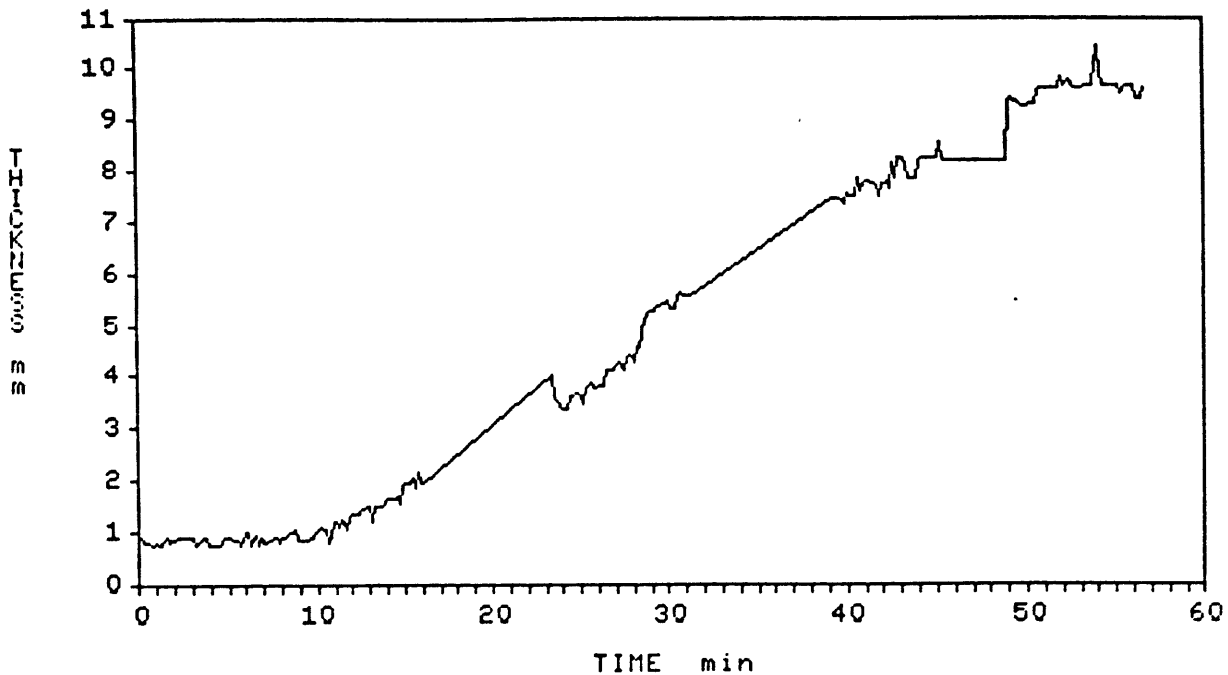
Flight 86-31 Using Algorithm 3

Figure 37: Ice Thickness vs. Time

Flight 86-32 Using Algorithm 3

Algorithm 3, the gated peak detector, worked well on the data from all three flights. Before comparing the results from Algorithm 3 with the analog results, one final algorithm is described.

Algorithm 4 attempts to minimize the small scale variations in the thickness measurements apparent in the previous plots. All three previous algorithms use only the first of the two waveforms that were stored every 10 seconds. Algorithm 4 averages the measurements from both waveforms. It uses the same gating routine as algorithm 3 and throws out waveforms with SNR's less than 1. If the SNR from one of the two waveforms is less than 1 then it

looks only at the other waveform. If both SNR's are less
than 1 then it keeps the previous measurement.   Figures
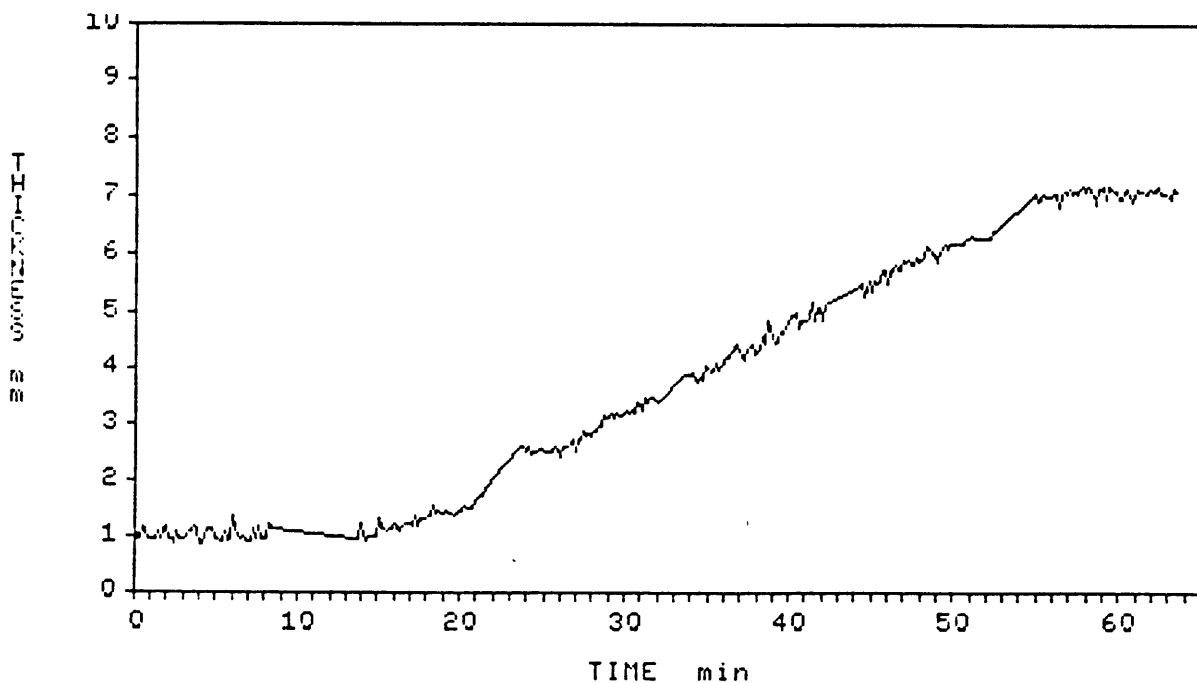38, 39 and 40 show the results using Algorithm 4.

Figure 38:   Ice Thickness vs. Time
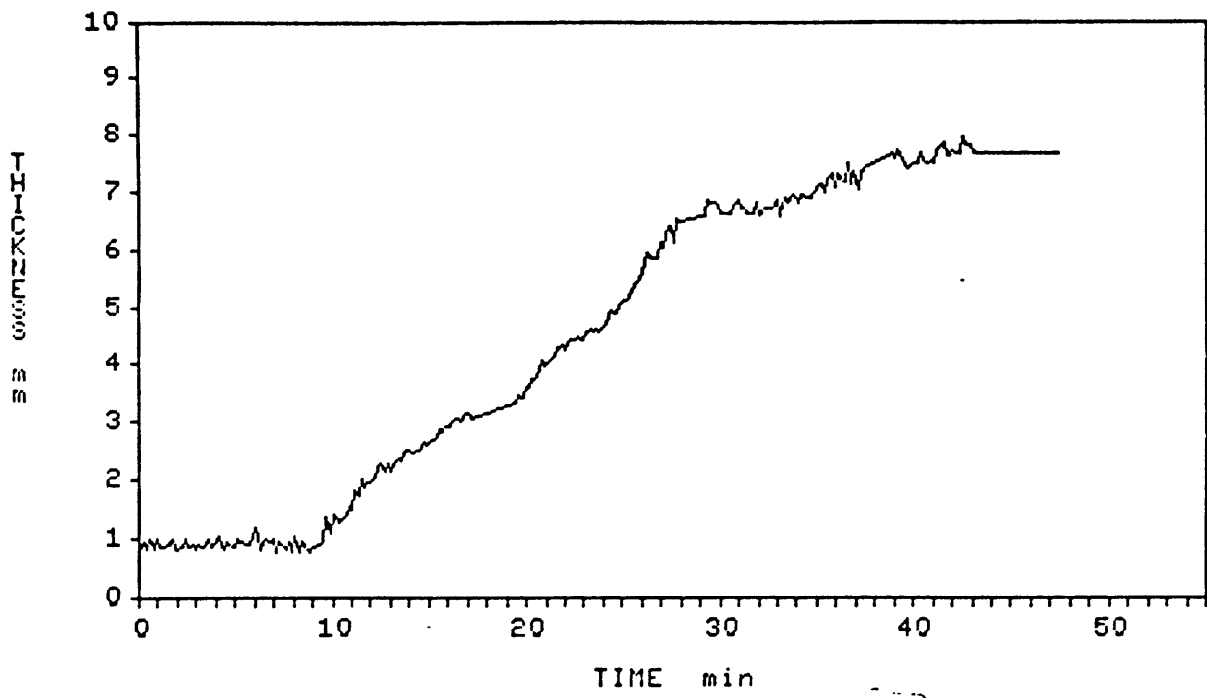
Flight 86-30 Using Algorithm 4

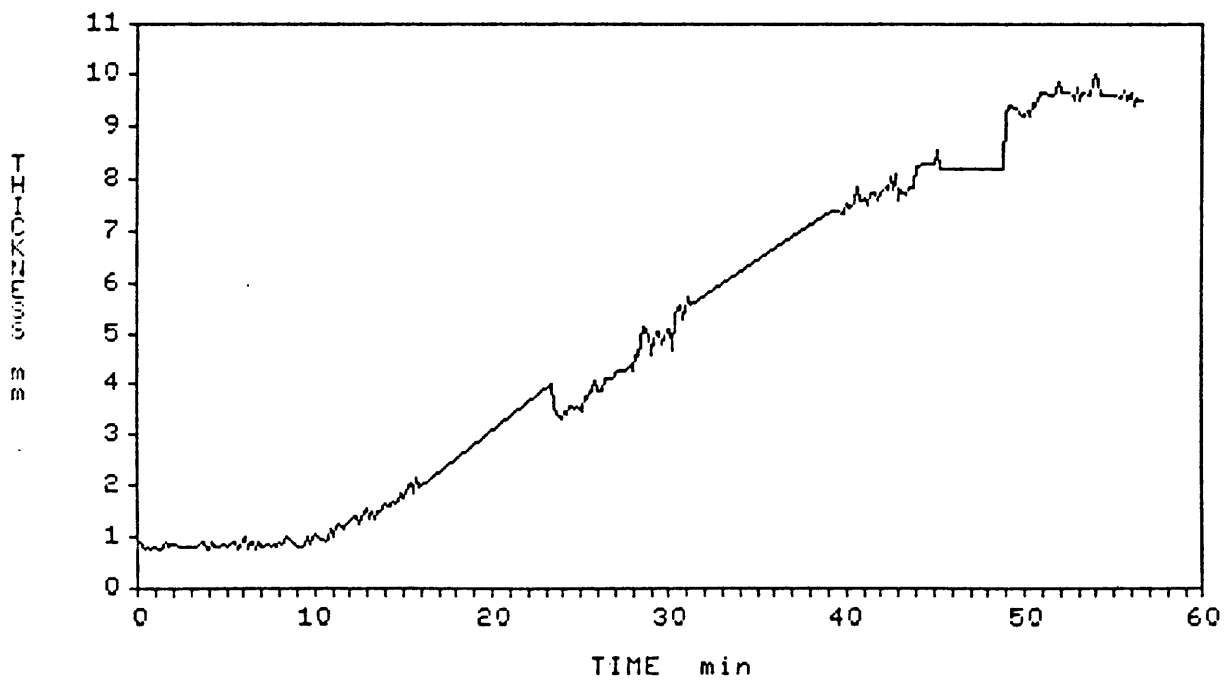Figure 39: Ice Thickness vs. Time

Flight 86-31 Using Algorithm 4

Figure 40: Ice Thickness vs. Time

Flight 86-32 Using Algorithm 4

Algorithm 4 was not a significant improvement over Algorithm 3, and the added computation time was not justified. Therefore, the results from Algorithm 3 were used for comparison with the analog data and for computation of the icing rate using the rate algorithms.

3.5 COMPARISON OF DIGITAL AND ANALOG RESULTS

The videotapes from the analog signal aquisition system were reduced manually. The thickness of the ice above each of the 8 transducers was determined from the oscilloscope traces at one or two minute intervals for Flights 86-30, 86-31, and 86-32. Data from the transducer closest to the digital transducer is presented for flights 86-31 and 86-32 (Figures 42 and 43) for comparison with the results from Algorithm 3. Some of the data from the closest transducer was lost during flight 86-30 due to an equipment malfunction so data from another array transducer is presented from that flight (Figure 41). Differences between the analog and digital ice thickness plots in Figure 40 are probably due to real variation in the ice thickness over the two transducers. The ice thickness measured mechanically at the end of each flight is also marked on Figures 41, 42, and 43.
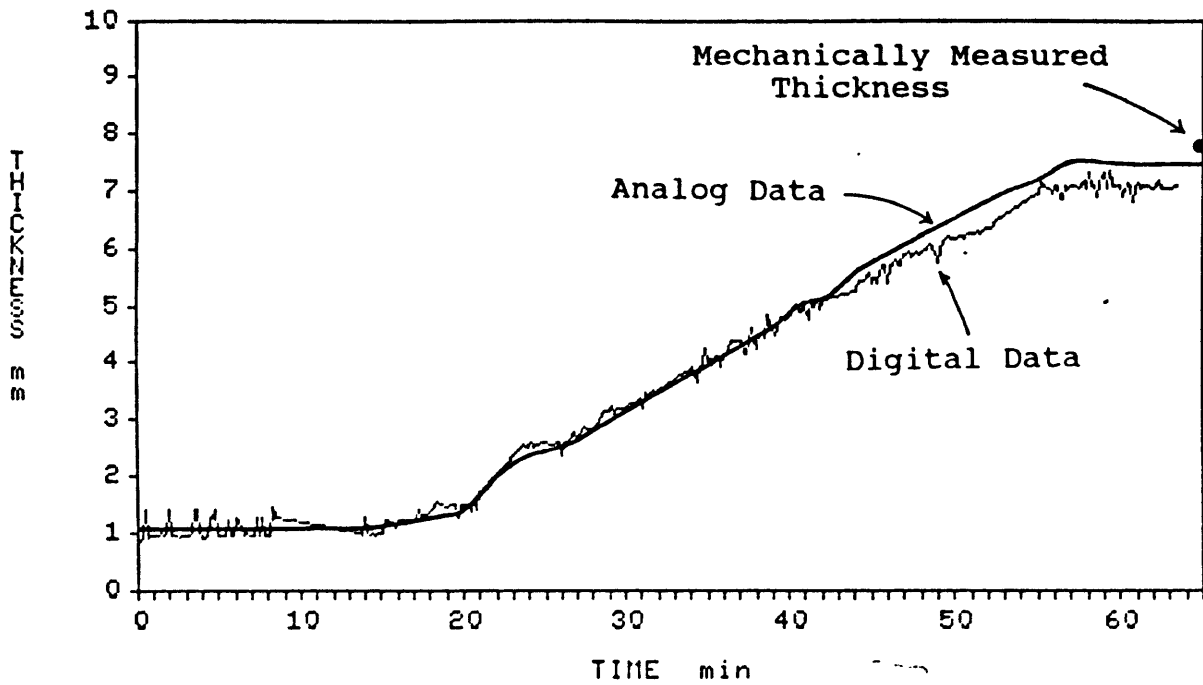
Figure 41: Ice Thickness vs. Time for Flight 86-30
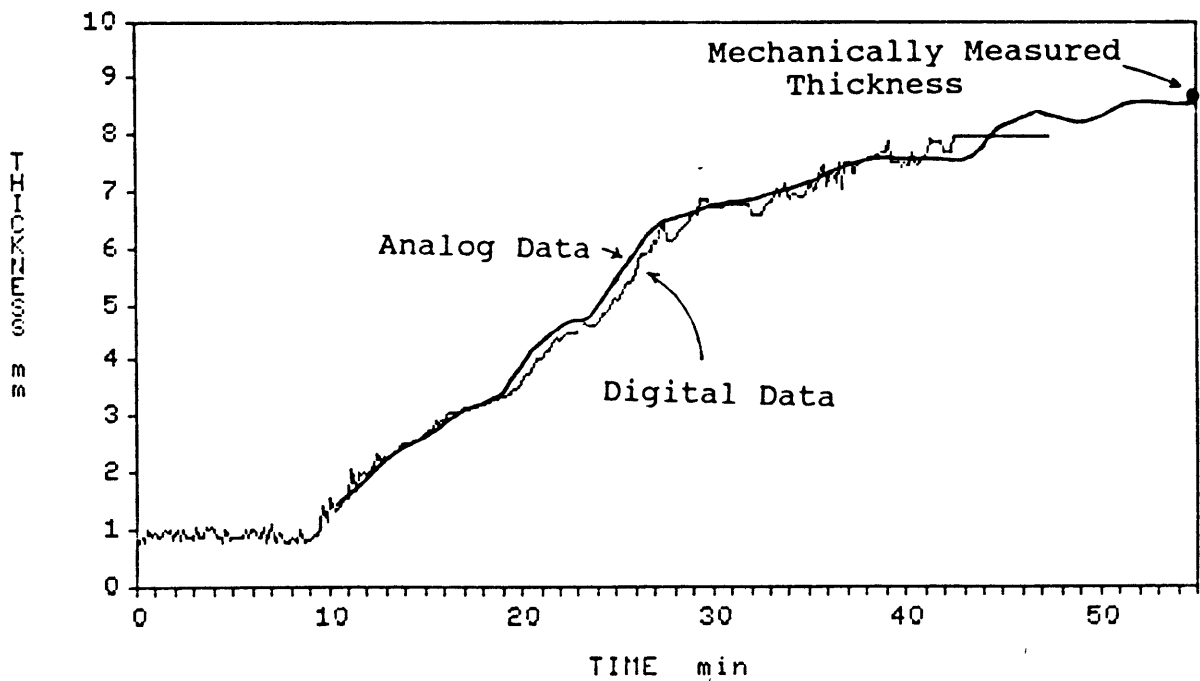
Comparison of Analog and Digital Data

Figure 42: Ice Thickness vs. Time for Flight 86-31
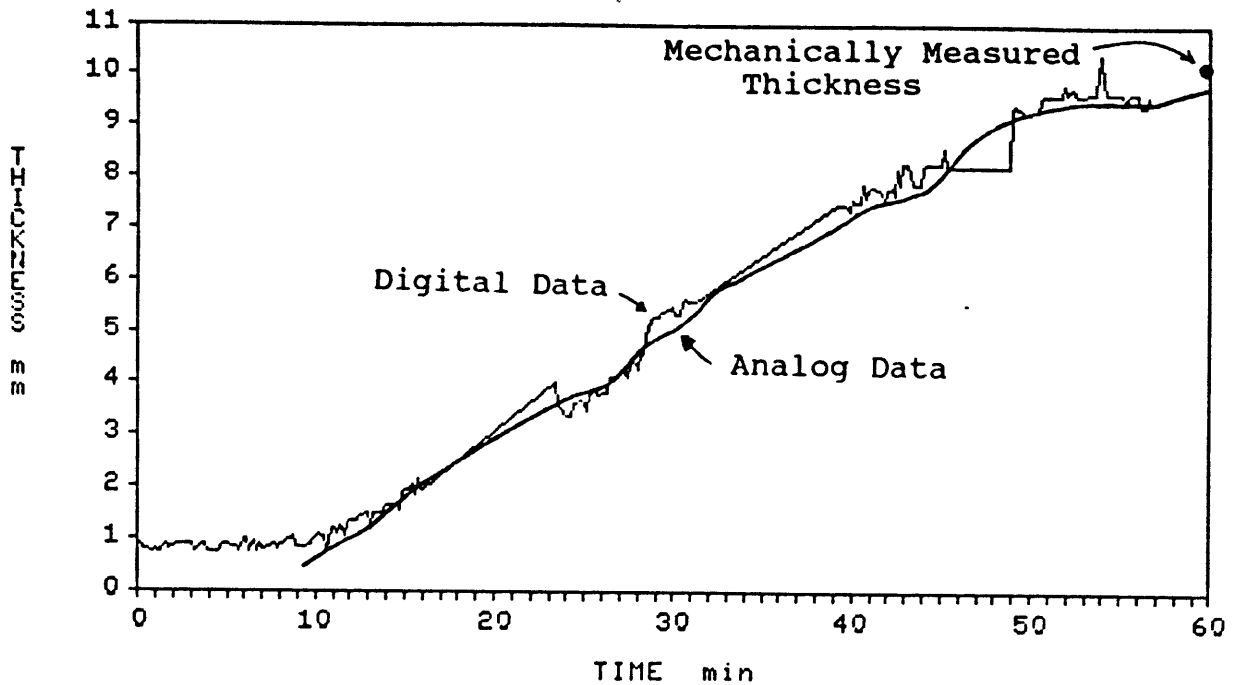
Comparison of Analog and Digital Data

Figure 43: Ice Thickness vs. Time for Flight 86-32
Comparison of Analog and Digital Data

The analog and digital results correlate well for all three flights. The final mechanical measurements are about 0.5 mm higher than the final digital and analog measurements. This difference is most likely due to a small amount of ice accretion between the final digital and analog measurements and the mechanical measurement (the mechanical measurement was taken up to 30 minutes after the final digital and analog measurements).

3.6 RATE ALGORITHMS

Three algorithms were developed to determine the icing rate from the thickness data presented in the previous section. All three compute the average rate over a specified period: Rate Algorithm 1 averages over 20 seconds (2 measurements), Rate Algorithm 2 averages over 50 seconds (5 measurements), and Rate Algorithm 3 averages over 2 minutes (12 measurements). Figures 44 to 55 show the results using the rate algorithms on the data from Thickness Algorithm 3. Thickness Algorithm 4 data was also tried but the results did not differ appreciably from the presented results. Plots of the liquid water content (LWC) measured during the three flights are shown for comparison with the icing rate determined by Rate Algorithm 3. Some correlation between the LWC and the icing rate was expected because all three flights were dry conditions, where nearly all the droplets freeze on impact.
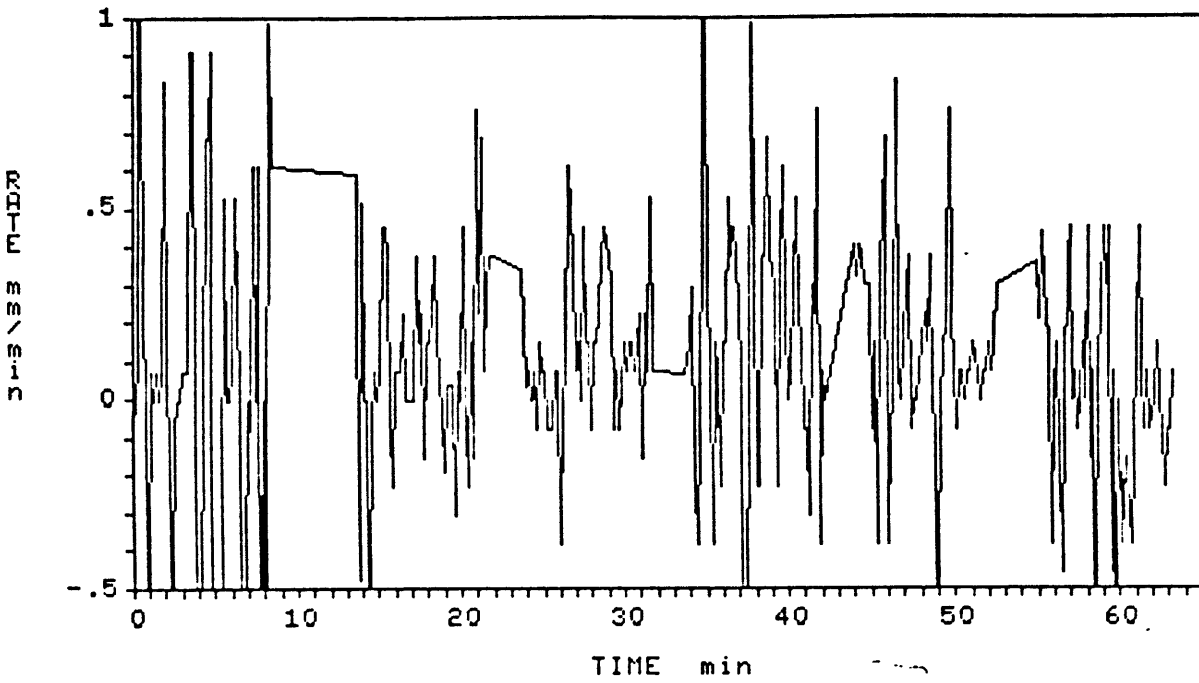
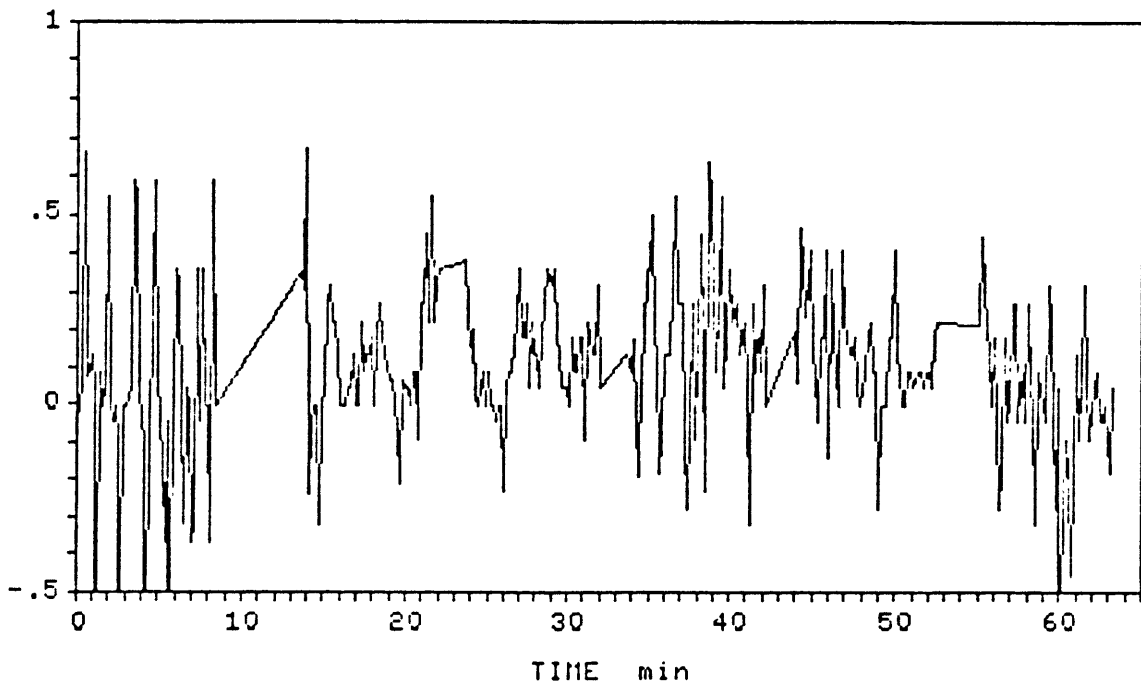**Figure 44: Icing Rate vs. Time**

Flight 86-30 Using Rate Algorithm 1

Figure 45: Icing Rate vs. Time
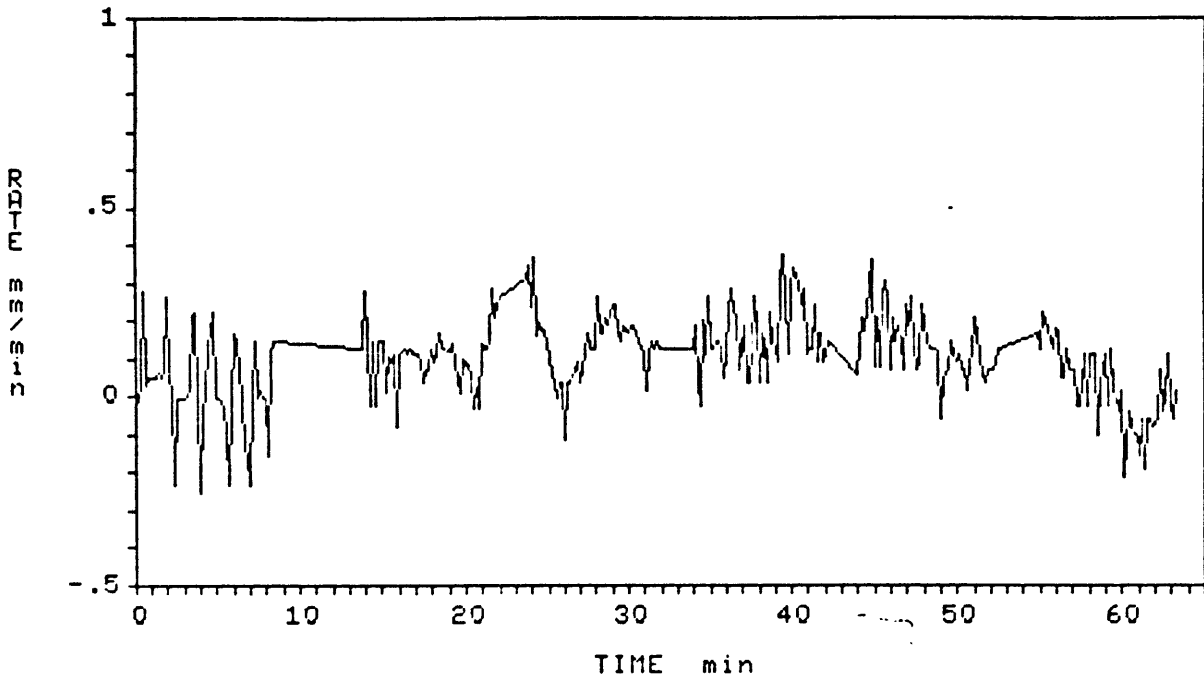
Flight 86-30 Using Rate Algorithm 2

Figure 46: Icing Rate vs. Time

Flight 86-30 Using Rate Algorithm 3

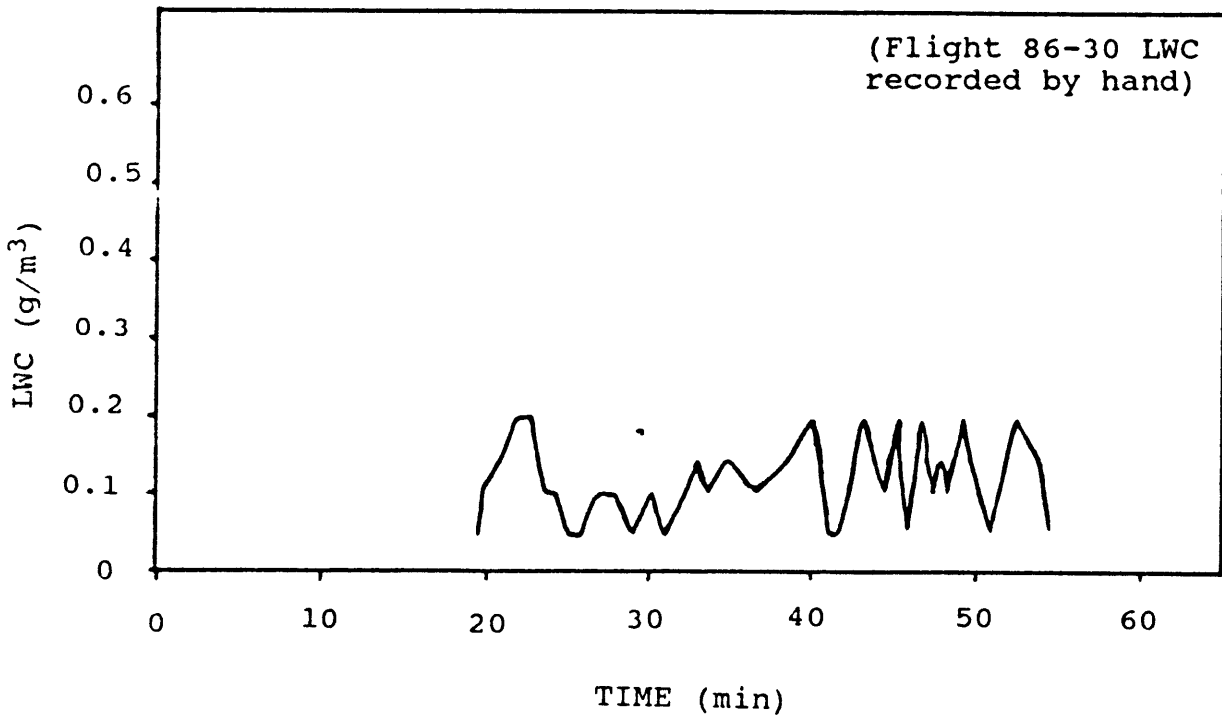(Flight 86-30 LWC recorded by hand)

Figure 47: Liquid Water Content vs. Time

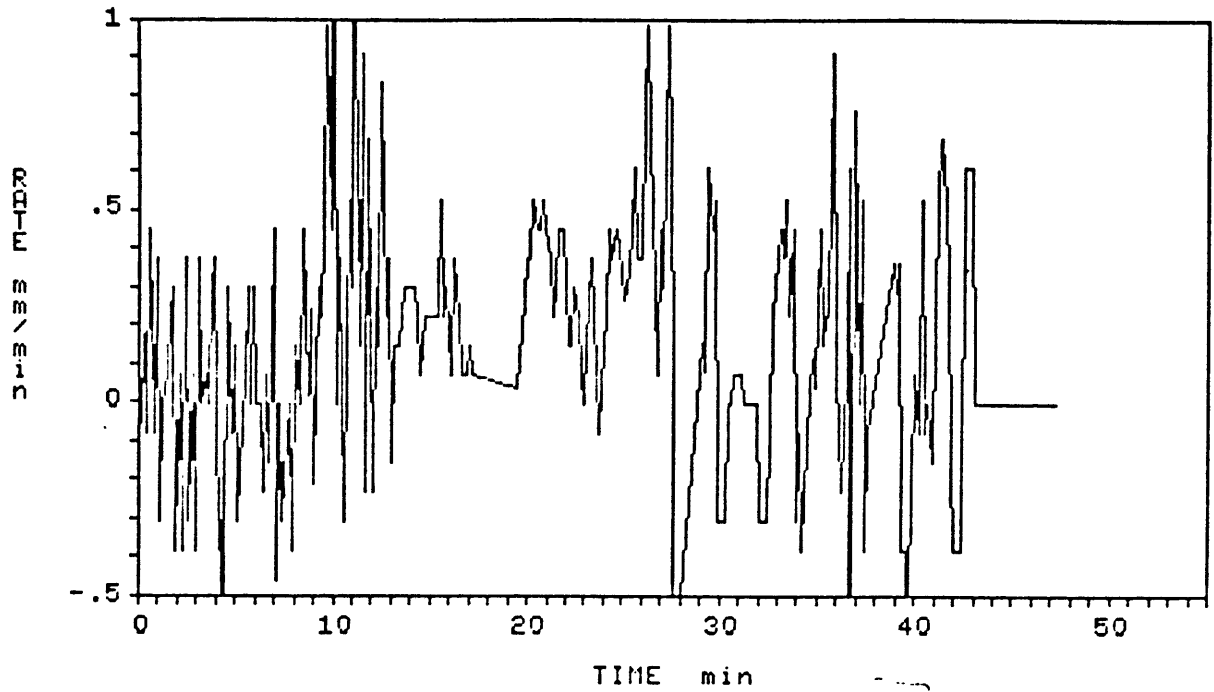Flight 86-30 Using Johnson-Williams Probe

Figure 48: Icing Rate vs. Time
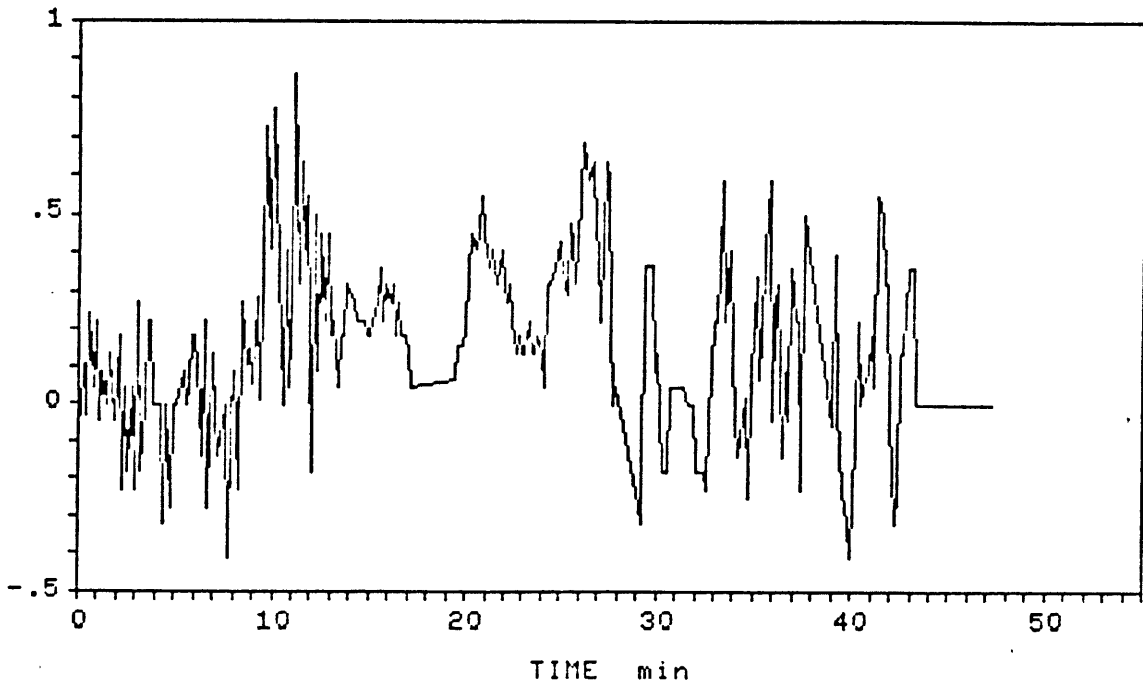
Flight 86-31 Using Rate Algorithm 1

Figure 49: Icing Rate vs. Time

Flight 86-31 Using Rate Algorithm 2

-67-

Figure 50:   Icing Rate vs. Time

Flight 86-31 Using Rate Algorithm 3

Figure 51:   Liquid Water Content vs. Time

Flight 86-31 Using Johnson-Williams Probe

Figure 52:   Icing Rate vs. Time

Flight 86-32 Using Rate Algorithm 1

Figure 53:   Icing Rate vs. Time

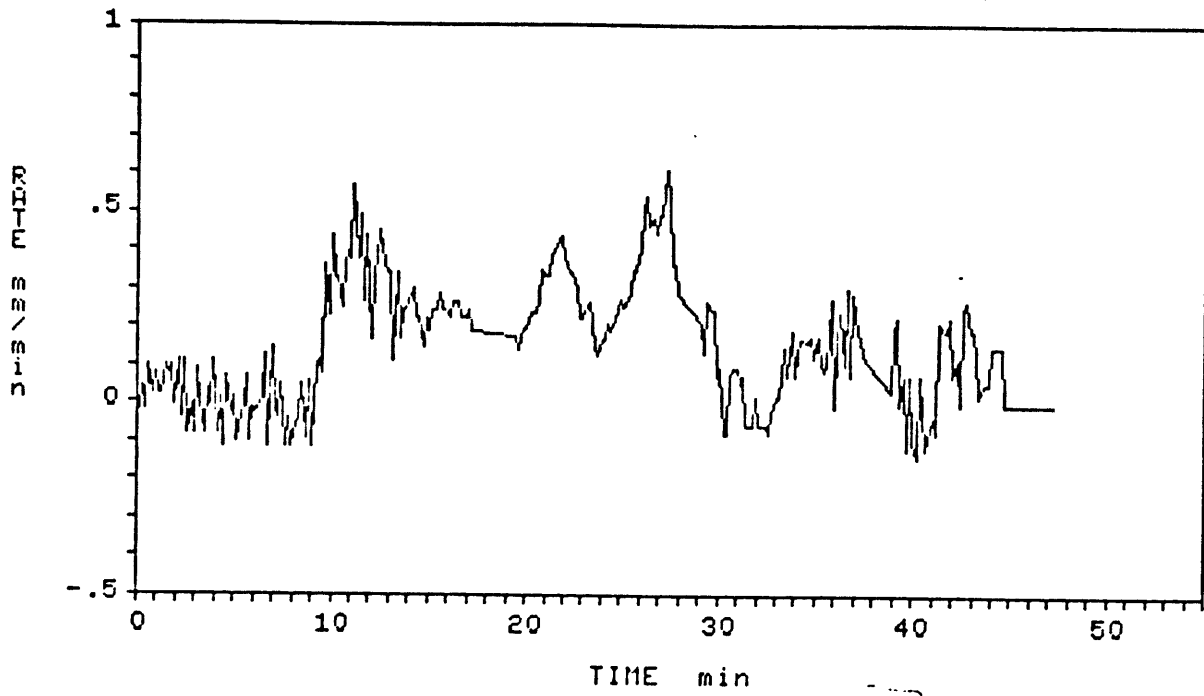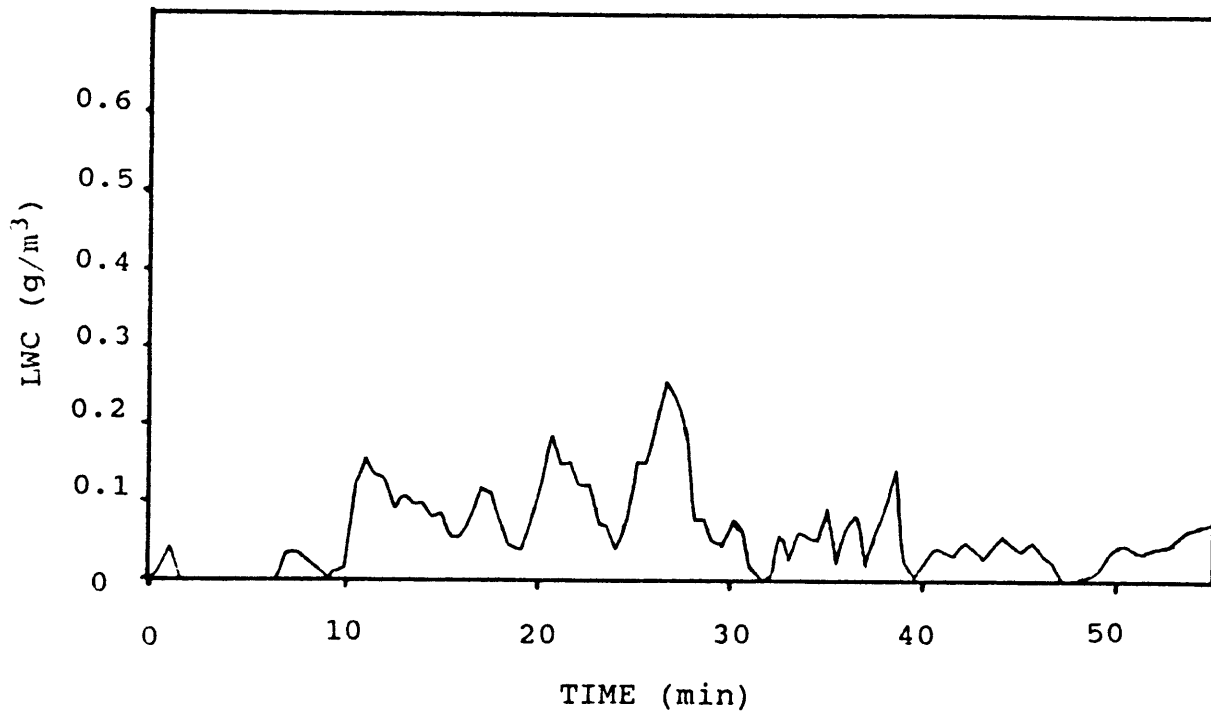Flight 86-32 Using Rate Algorithm 2

-69-
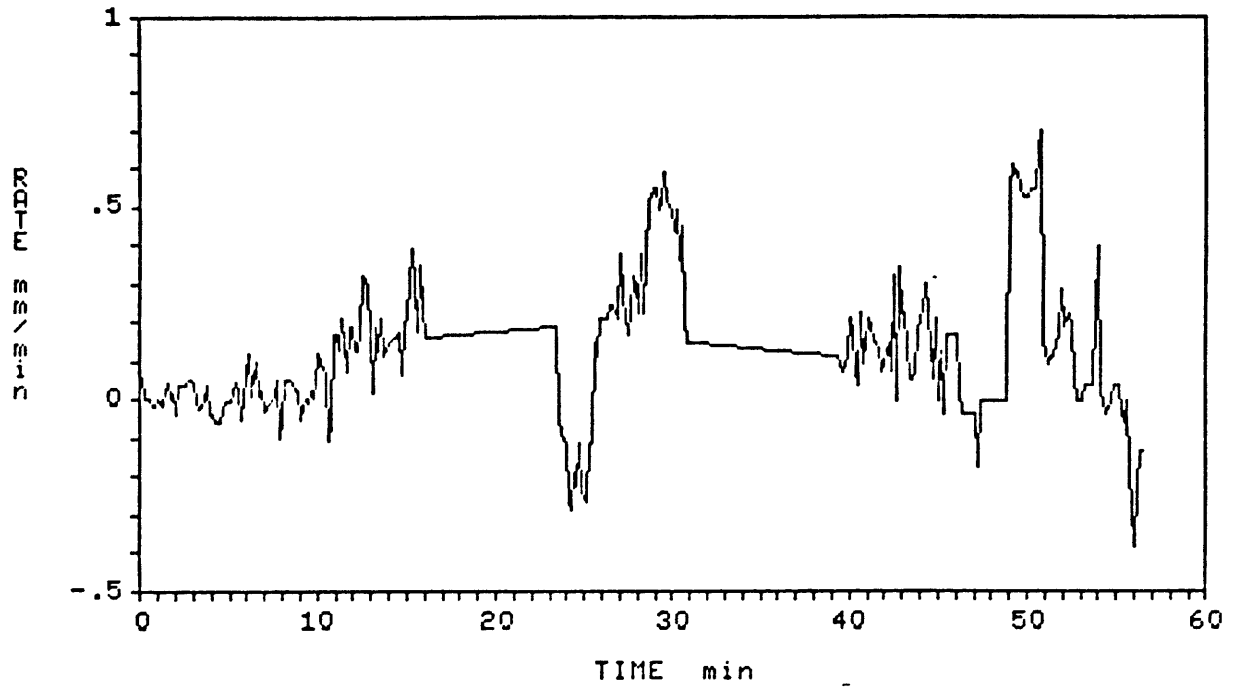
Figure 54:   Icing Rate vs. Time

Flight 86-32 Using Rate Algorithm 3
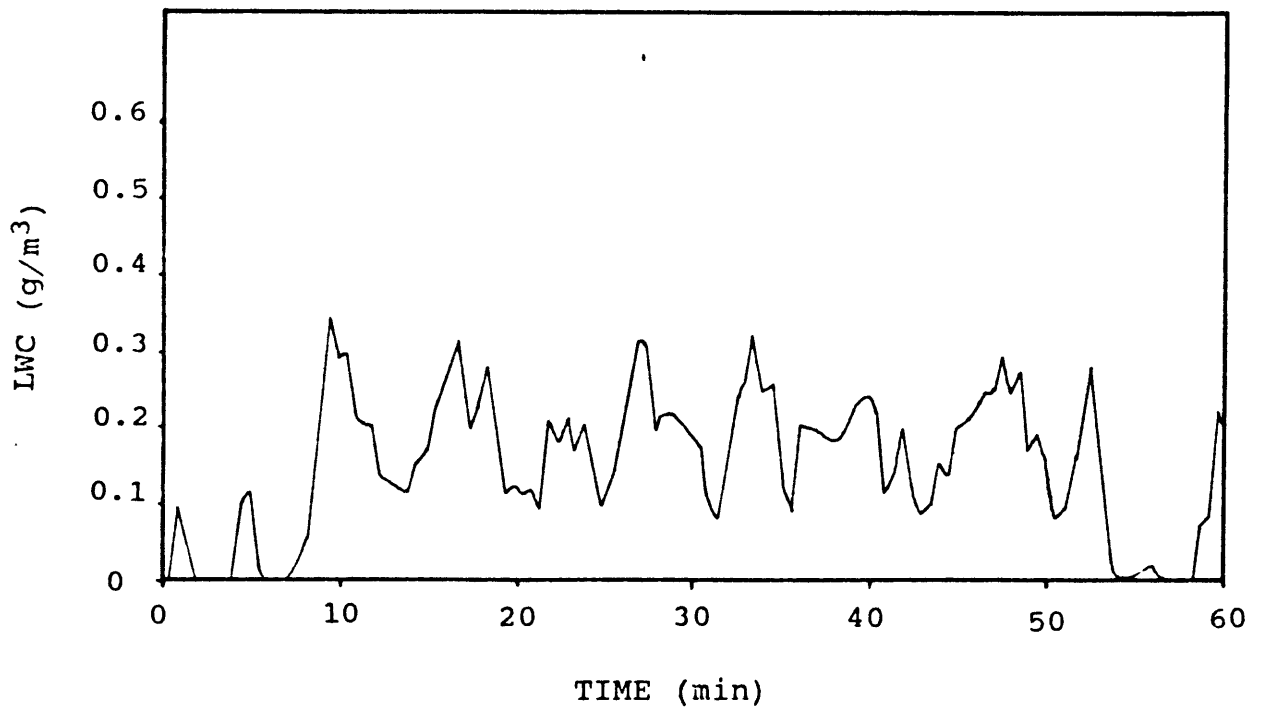
Figure 55:   Liquid Water Content vs. Time

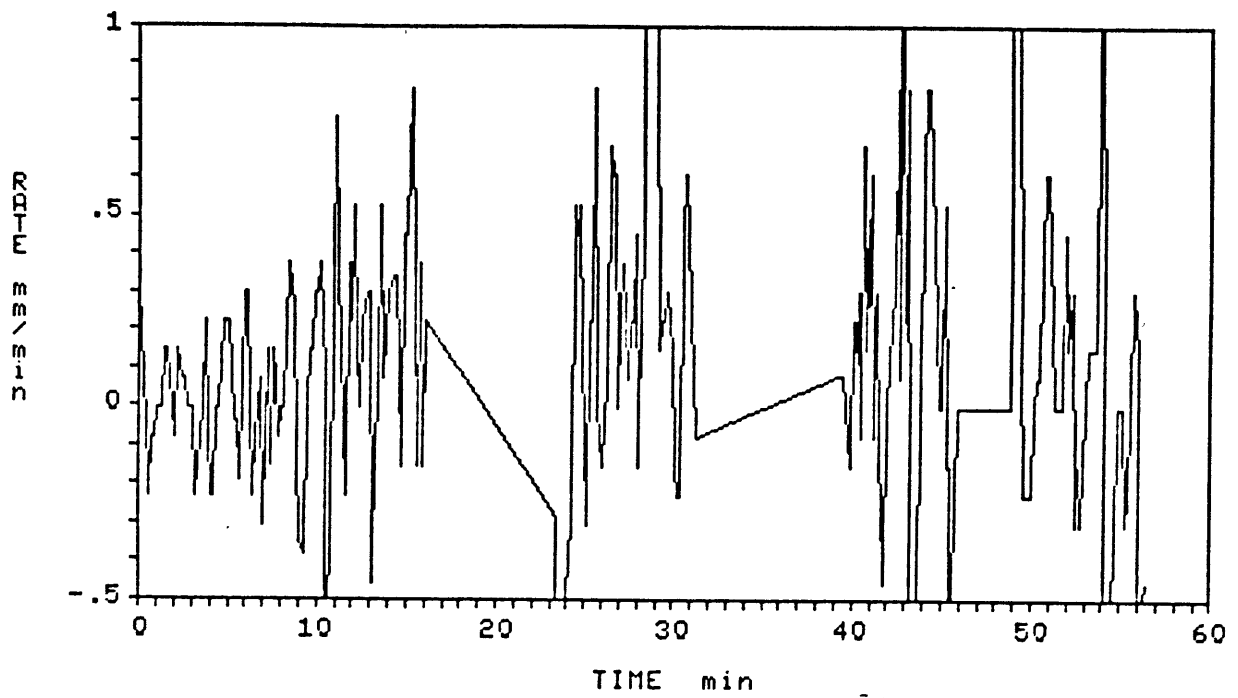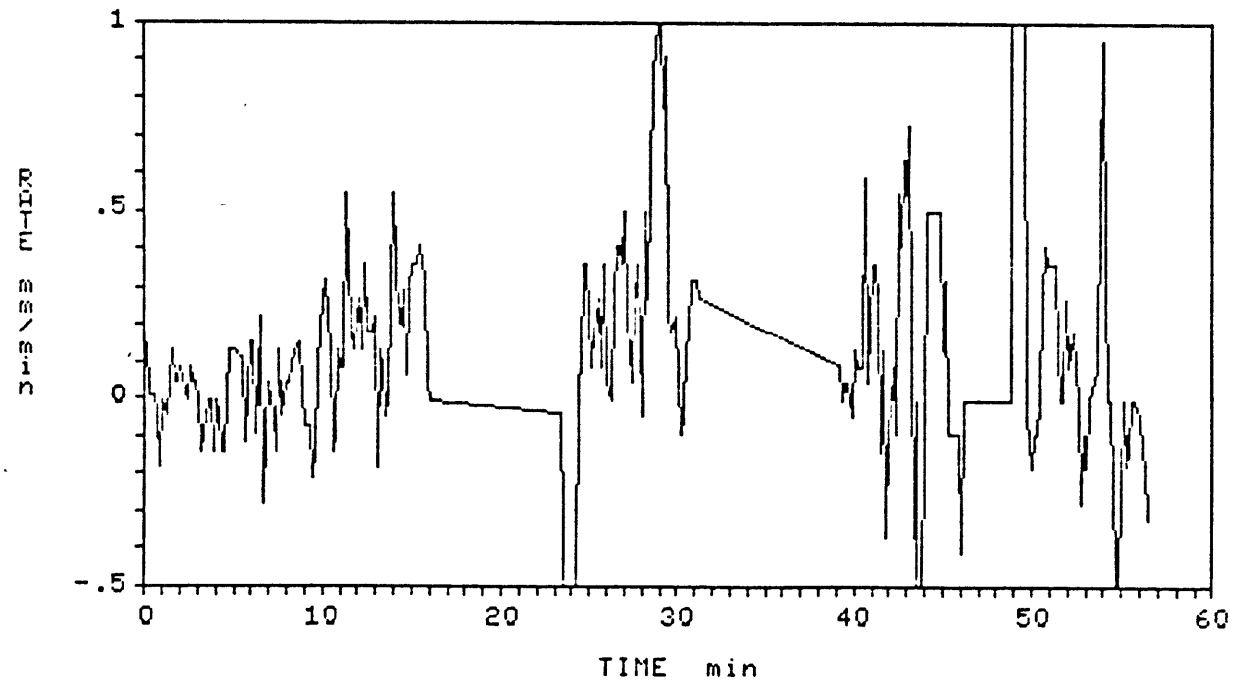Flight 86-32 Using Johnson-Williams Probe

The icing rate algorithms did not work as well as the thickness algorithms. Since all three flights showed relatively low icing rates, a large number of measurements was required to determine the icing rate. Even with 2 minute averaging, a large amount of noise was present in the rate data. Improved icing rate performance could probably be achived by storing a larger number of waveforms at each time interval and then averaging (i.e. average 8 closely spaced measurements at 10 second intervals).

4. CONCLUSIONS

The following conclusions were drawn from the flight tests and the signal processing results:

1. Digital acquisition of the ultrasonic signals provided a useful data set for evaluating signal processing algorithms.

2. The gain of the receiver is a sensitive parameter, so that automatic gain control would be useful in future systems.

3. Preprocessing of the waveforms using a derivative approximation provides a method for finding a consistent point in the ice/air echo. It also improves the signal to noise ratio.

4. Signal processing algorithms employing simple peak detection to find the ice/air echo tend to fail when the signal to noise ratio is low or layers are present in the ice.

5. The most successful algorithm developed for determining the ice thickness employes a gated peak detector and low SNR filtering. This algorithm correctly measured the ice thickness for the three flights tested. It could be implemented using either

digital or analog techniques.

6. The results from icing rate measurement algorithms correlated reasonably well with liquid water content measurements. The icing rate measurements contained a large amount of noise and required a long averaging period (2 minutes). Increasing the number of thickness measurements would most likely reduce the noise in the icing rate measurements and decrease the averaging period required.

7. An operational instrument employing digital acquisition and processing is feasible, but may not be necessary. The processing algorithms developed could be used in an analog system.

APPENDIX A: EQUIPMENT SPECIFICATIONS

Transducers -   Panametrics, Inc. Model M201-RM, 5.0
                        Mhz center frequency, broadband, 1/4
                        inch diameter transducers with Model
                        DLH-1, 10 microsecond plexiglass delay
                        line.

Pulser-Receiver - Panametrics, Inc. Model 5055 pulser-
                        receiver.

Tape Deck -   Analog and Digital Peripherals, Inc.
                        Model LG-2-P, 8-bit parallel
                        minicassette tape recorder. Phillips
                        digital minicassettes.

APPENDIX B: REFERENCES

1. Hansman, R.J. and Kirby, M.S., "Measurement of Ice Accretion Using Ultrasonic Pulse-Echo Techniques," *Journal of Aircraft*, Vol. 22, June 1985, pp. 530-535.

2. Hansman, R.J. and Kirby, M.S., "Real-Time Measurement of Ice Growth During Simulated and Natural Icing Conditions Using Ultrasonic Pulse-Echo Techniques," AIAA 86-0410, 1986.

3. Ide, R.F. and Richter, G.P., "Comparison of Icing Cloud Instruments for 1982-1983 Icing Season Flight Program," NASA-TM-83569, 1984.

4. Perkins, P.J., McCullough, S., and Lewis, R.D., "A Simplified Instrument for Recording and Indicating Frequency and Intensity of Icing Conditions Encountered in Flight," NACA RM-E51E16, 1951.

5. Brun, R.J., Lewis, W., Perkins, P.J., and Serafini, J.S., "Impingement of Cloud Droplets on a Cylinder and Procedure for Measuring Liquid-Water Content and Droplet Sizes in Super Cooled Clouds by Rotating Multicylinder Method," NACA Rep. 1215, 1955.

6. Watson, D., "At Video Bandwidths, Flash A-D Converters Dictate Stringent Design," *Electronic Design*, June 6, 1985, pp. 143-148.

7. Muramatsu, J. and Olsen, R.K., "6-Bit A-D Chip Steps Up the Pace of Signal Processing", *Electronic Design*, Sept 16, 1982.

8. Comlinear Corporation, CLC300A Technical Data Sheet and AN200-1 Application Note.

9. Cypress Semiconductor Corporation, CMOS Data Book, CY7C128-35, pp. 2-16 to 2-21.